Front. Struct. Civ. Eng. 2022, 16(7): 817–842
https://doi.org/10.1007/s11709-022-0844-y

RESEARCH ARTICLE

Axial compression tests and numerical simulation of steel reinforced recycled concrete short columns confined by carbon fiber reinforced plastics strips

Hui MA[a,b*], Fangda LIU[b], Yanan WU[b], Xin A[c,d], Yanli ZHAO[b]

[a] *State Key Laboratory of Eco-hydraulics in Northwest Arid Region, Xi'an University of Technology, Xi'an 710048, China*
[b] *School of Civil Engineering and Architecture, Xi'an University of Technology, Xi'an 710048, China*
[c] *Qinghai Building and Materials Research Co., Ltd, Xining 810008, China*
[d] *Qinghai Provincial Key Laboratory of Plateau Green Building and Eco-community, Xining 810008, China*
[*] *Corresponding author. E-mail: mahuiwell@163.com*

ABSTRACT To research the axial compression behavior of steel reinforced recycled concrete (SRRC) short columns confined by carbon fiber reinforced plastics (CFRP) strips, nine scaled specimens of SRRC short columns were fabricated and tested under axial compression loading. Subsequently, the failure process and failure modes were observed, and load-displacement curves as well as the strain of various materials were analyzed. The effects on the substitution percentage of recycled coarse aggregate (RCA), width of CFRP strips, spacing of CFRP strips and strength of recycled aggregate concrete (RAC) on the axial compression properties of columns were also analyzed in the experimental investigation. Furthermore, the finite element model of columns which can consider the adverse influence of RCA and the constraint effect of CFRP strips was founded by ABAQUS software and the nonlinear parameter analysis of columns was also implemented in this study. The results show that the first to reach the yield state was the profile steel in the columns, then the longitudinal rebars and stirrups yielded successively, and finally RAC was crushed as well as the CFRP strips was also broken. The replacement rate of RCA has little effect on the columns, and with the substitution rate of RCA from 0 to 100%, the bearing capacity of columns decreased by only 4.8%. Increasing the CFRP strips width or decreasing the CFRP strips spacing could enhance the axial bearing capacity of columns, the maximum increase was 10.5% or 11.4%, and the ductility of columns was significantly enhanced. Obviously, CFRP strips are conducive to enhance the axial bearing capacity and deformation capacity of columns. On this basis, considering the restraint effect of CFRP strips and the adverse effects of RCA, the revised formulas for calculating the axial bearing capacity of SRRC short columns confined by CFRP strips were proposed.

KEYWORDS steel reinforced recycled concrete, CFRP strips, short columns, axial compression behavior, recycled aggregate concrete

1 Introduction

The waste concrete is crushed to form coarse aggregate and it is added into the concrete to form recycled aggregate concrete (RAC), which can not only protect the natural environment, but also reduce the consumption of building industrial materials and save the non-renewable stones, which is in line with the development requirements of green buildings in the world [1–4]. At present, the mechanical properties of RAC material and its structure had been widely studied and preliminarily applied in engineering all over the world [5–6]. Most of the research results indicate that the physical mechanics performance of RAC is slightly lower than that of normal concrete, but it still can be used in the building structure through the reasonable design and construction [7–11]. Therefore, the application of RAC material can solve the impact of construction waste on the environment and is of

Article history: Received Oct 18, 2021; Accepted Mar 21, 2022

great significance to the green development of construction industry.

Nevertheless, in order to develop the engineering application of RAC, improving the mechanical properties of RAC and its structure is still one of the current research focuses. Some scholars combined RAC with profile steel to form steel reinforced recycled concrete (SRRC) composite members, and studied their mechanical properties [12–14], so as to enhance the mechanical properties of RAC structures and components. The results show that profile steel used in the RAC structural components can effectively enhance the mechanical properties of RAC structure. Even so, compared with natural concrete, the use of RAC has a certain impact on the deformation capacity and axial bearing capacity of SRRC columns. Moreover, in order to enhance the vertical bearing capacity of SRRC members, some scholars had also researched the mechanical performance of SRRC filled steel tube columns [15–20]. The results show that the steel tube has good restraint capacity to the SRRC columns, which can greatly enhance the vertical bearing capacity of columns, and this kind of composite column also shows good ductility and deformation ability. However, it is not economical to adopt the steel tube to enhance the mechanical properties of SRRC columns, mainly because the large amount of steel material leads to the increase of construction cost. In addition, when exposed to the external environment, the steel tube is prone to rust and the durability as well as the service performance of structural members is reduced.

Fortunately, as a kind of reinforcing material in the field of civil engineering, carbon fiber reinforced plastics (CFRP) material has high tensile strength, good durability and appropriate cost. Therefore, it is widely used in the engineering field, mainly used for restraining and strengthening components in the engineering structures. In view of the good restraint effect of CFRP material, many scholars have applied it in reinforced concrete, so as to improve the performance of reinforced concrete components and structures. It indicates that the reinforced concrete is compressed in three directions under the strong restraint of CFRP, which can not only significantly enhance the bearing capacity of reinforced concrete, but also improve its deformation capacity [21–24]. In addition, CFRP tube can also improve the compression properties of RAC columns, and the replacement percentage of recycled coarse aggregate (RCA) has no great impact on the restraint effect of CFRP [25].

In view of this, CFRP strips were adopted to enhance the mechanical properties of SRRC columns. At present, there are few reports on the research of SRRC columns confined by CFRP strips, so it needs to be studied. In this study, nine scaled specimens of SRRC short columns confined by CFRP strips were made and experimented under axial compression loading. The effects of the replacement rate of RCA, CFRP strips spacing, CFRP strips width and RAC strength on the axial compression properties of members were investigated in detail. Furthermore, the nonlinear mechanical behavior and parametric analysis of SRRC short columns confined by CFRP strips under axial compression loading was also studied. Based on the above research, the revised calculation method of SRRC short columns confined by CFRP strips under the axial bearing capacity was proposed in this study, and its effectiveness was determined through experimental comparison, which provided a reference for engineering application.

2 Experimental investigation of SRRC short columns confined by carbon fiber reinforced plastics strips

2.1 Design and manufacture of specimens

Nine scaled (1:3) test specimens of SRRC short columns confined by CFRP strips were designed and manufactured in this experimental investigation. The test design parameters of specimens such as the replacement rate of RCA, CFRP strips spacing, CFRP strips width and RAC strength were mainly considered. See Table 1 for the basic parameters of the specimens. The geometric sizes and section form of specimens are shown in Fig. 1.

Three strength levels of RAC (i.e., C40, C50, and C60) were designed and prepared in the test. The RCA used in the specimens came from the waste concrete of disused building, with a continuous grading of 5–25 mm, and it was made by crushing, screening, cleaning, drying and other processes. The basic performance of RCA can satisfy the use stipulation of "recycled coarse aggregate for concrete" (GB/T-25177-2010 , in China) [26]. Figure 2 shows the RCA and test cubes of RAC in the test. Tables 2 and 3 show the mix proportion design and basic performance indexes of RAC material, respectively.

The profile steel used in the specimens was the hot rolled profile steel with the strength grade of Q235, and the section size was 140 mm × 80 mm × 5.5 mm. HRB400 hot-rolled rebars were adopted in the test specimens, and the diameters of longitudinal rebars and stirrups were 16 and 8 mm, respectively. Table 4 shows the basic mechanical performance of steel in the specimens. Moreover, the CFRP material adopted in this test were produced by Fischer Company in Germany, and the basic performance indexes of CFRP are listed in Table 5. In order to learn the influence of CFRP strips width on the behavior of SRRC columns, CFRP strips width in the specimens were 35, 50, and 65 mm, respectively according to literature [27]. Figure 3 shows the construction process of CFRP strips on the specimens of columns.

Table 1 Basic design parameters on the specimens of columns

specimen number	column height L (mm)	replacement rate of RCA r	RAC strength	CFRP strips width b (mm)	CFRP strips spacing s (mm)	wrapping layers of CFRP strips n
CFRP-SRRC-1	500	0%	C40	50	40	2
CFRP-SRRC-2	500	50%	C40	50	40	2
CFRP-SRRC-3	500	100%	C40	50	40	2
CFRP-SRRC-4	500	100%	C40	50	50	2
CFRP-SRRC-5	500	100%	C40	50	25	2
CFRP-SRRC-6	500	100%	C40	65	40	2
CFRP-SRRC-7	500	100%	C40	35	40	2
CFRP-SRRC-8	500	100%	C50	50	40	2
CFRP-SRRC-9	500	100%	C60	50	40	2

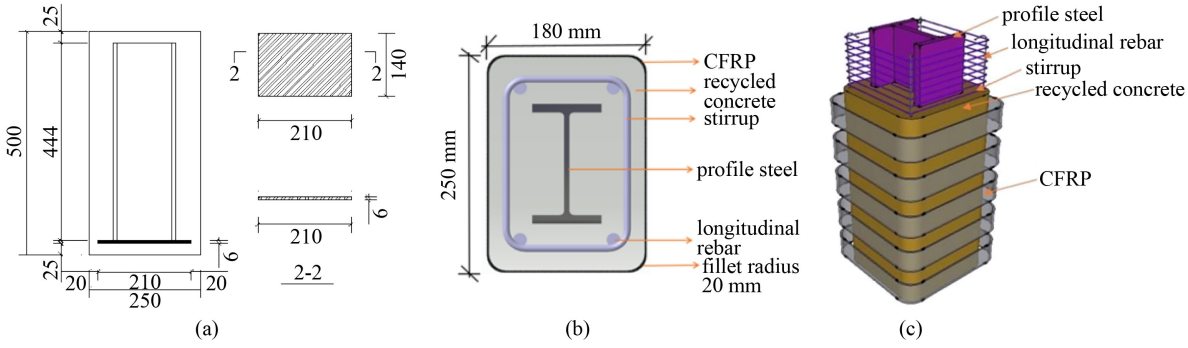

Fig. 1 Geometrical dimension and section form of specimens: (a) geometric dimension; (b) cross section; (c) composition features.

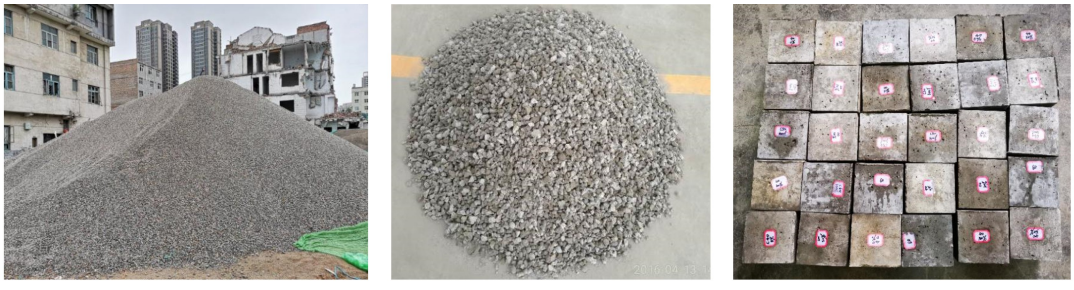

Fig. 2 RCA and test cubes of RAC in the specimens. (a) RCA material field; (b) RCA product; (c) RAC cube.

Table 2 Mixture ratio of RAC material

strength of RAC	water binder ratio	replacement rate of RCA	unit volume consumption (kg/m^3)						
			fly ash	natural coarse aggregate	river sand	water reducing agent	recycled coarse aggregate	cement	water
C60	0.312	100%	105	0	2.79	6.30	48.01	422	164.5
C50	0.360	100%	94	0	2.76	4.78	45.69	358	163.0
C40	0.512	100%	0	0	2.68	1.75	43.01	443	226.8
	0.476	50%	0	585.5	2.90	1.75	53.05	443	210.9
	0.411	0	0	1171	3.03	1.75	60.69	443	182.1

When making the test specimens, the longitudinal rebars and stirrups were assembled to form the reinforcement skeletons, and they were welded together with the profile steel through the bottom plate to fix the position of profile steel and reinforcement skeletons. Then the wooden formwork of specimens was set up and the mixture of RAC material shall be evenly mixed and vibrated during pouring. Figure 4 shows the main

Table 3 Basic mechanical performance of RAC

strength of RAC	water binder ratio	replacement rate of RCA	axial compressive strength f_{rc} (MPa)	elastic modulus E_{rc} (10^4 MPa)	tensile strength f_{rt} (MPa)	cubic compressive strength f_{rcu} (MPa)
C60	0.312	100%	46.13	3.03	2.78	60.69
C50	0.36	100%	40.32	2.90	2.54	53.05
C40	0.512	100%	32.69	2.68	2.21	43.01
	0.476	50%	34.73	2.76	2.30	45.69
	0.411	0	36.49	2.79	2.38	48.01

Table 4 Basic mechanical performance of profile steel and rebars

steel types	yield strength f_y (MPa)	ultimate strength f_u (MPa)	elastic modulus E_s (MPa)	yield strain $\mu\varepsilon$
profile steel				
steel web	294.6	367.1	2.04×10^5	1444
steel flange	374.7	467.6	2.01×10^5	1864
longitudinal rebars (HRB400)	579.6	794	2.16×10^5	2683
stirrups (HRB400)	459.3	645	2.10×10^5	2187

Table 5 Basic performance indexes of CFRP material

type of CRFP	calculated thickness (mm)	tensile modulus of elasticity (MPa)	mass perunit area (g/m^2)	rate of elongation (%)	tensile strength (MPa)
FRS-CS-300	0.167	2.4×10^5	299.1	1.7	3565.2

(a) (b) (c)

Fig. 3 Construction process of CFRP strips for the specimens: (a) cutting of CFRP; (b) RAC surface polishing; (c) sticking of CFRP strips.

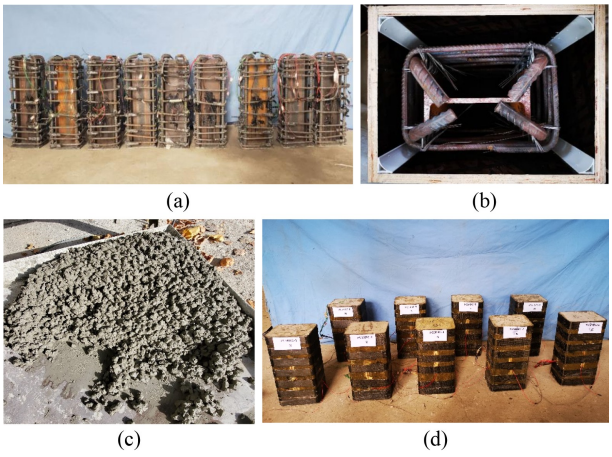

(a) (b) (c) (d)

Fig. 4 Main manufacturing process of specimens: (a) steel skeletons; (b) templates installing; (c) RAC pouring; (d) test specimens.

fabrication process of SRRC short columns confined by CFRP strips.

2.2 Test loading devices and measuring points

In this research, the axial loading test of specimens was carried out through using a 500 t electro-hydraulic servo press machine and the loading devices are shown in Fig. 5. To understand the failure process of columns under axial compression loading, the mixed loading procedure of force control and displacement control was used in the test. The main loading steps of experiment were described in detail as follows: 1) the specimen was preloaded before the formal loading and then unloaded to zero, so as to eliminate the clearance between the loading devices and specimen; 2) before the loads reached 80% of the estimated maximum bearing capacity, the force

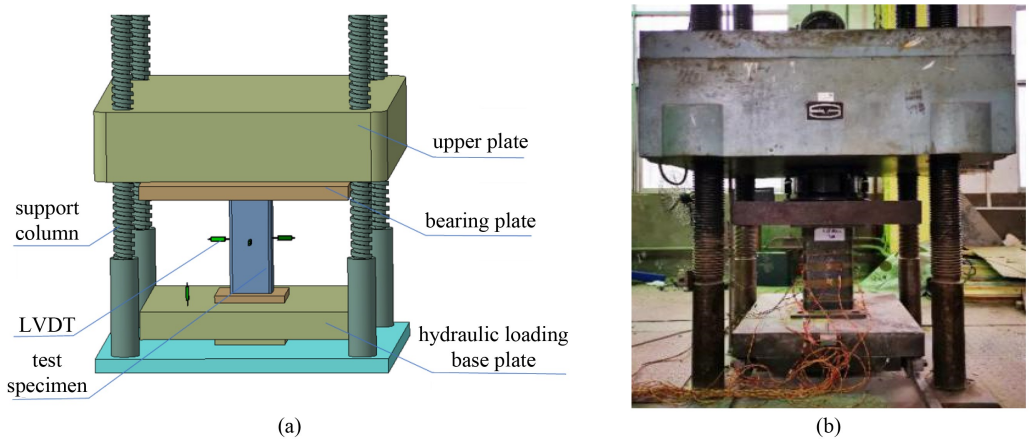

Fig. 5 Test loading devices and site photos of specimens: (a) test loading devices; (b) photos of test loading.

control was adopted, and each level of force was 1/15 of the estimated peak loads, and the loading duration of each load level was 1.0 min; 3) when the loads increased slowly, the loading procedure was changed to the displacement control, and load at the speed of 1.0 mm/min. When the axial bearing capacity of specimen decreased to 85% of the peak loads or specimen was deformed greatly and should not be loaded, which means that the specimen was seriously damaged and the axial compression test can be stopped.

Figure 6 shows the measuring points of strains and displacement meters of specimens in this study. Four transverse strain gauges were attached to the CFRP strips in the middle of the specimens to test the strain of CFRP. The vertical strain gauges were also attached to the longitudinal rebars and stirrups, respectively, so as to measure their strain development. And three longitudinal strain gauges were set in the middle of flange and web to monitor the strain law of profile steel. Moreover, four displacement meters perpendicular to the middle surface of specimens were arranged to measure the lateral displacement of specimens. One displacement meter was also arranged at the bottom of specimens to measure the relative vertical displacement of specimens.

3 Analysis of test results

3.1 Failure process and characteristics

Based on the observation of test process, the failure process and characteristics of SRRC short columns confined by CFRP strips under axial compression loading with different design parameters were basically similar. At the beginning of loading, the change of specimens was not obvious due to the small axial forces, and it was in the elastic state. When the axial force reached about 50% of peak load, there was a slight slip between CFRP strips and RAC, accompanied by a slight crisp sound. At the same time, a trivia crack appeared in RAC at the corner of specimens. As the axial load continued, some new cracks appeared one after another on the surface of specimens, and some original cracks at the corner gradually extended to the middle of specimens, and the click sound was constantly generated. When the axial force increased to about 80% of peak load, some CFRP strips on the specimens appeared the bulging deformation and their strains increased rapidly due to the axial compression loads. Meanwhile, more crevices appeared on the surface of RAC and the original crevices continued to extend, and the load-displacement curves of specimens were obviously nonlinear characteristics. It shows that the elastoplastic state of the columns had arrived. When the load of specimens was reached the peak load, some CFRP strips were gradually broken at the corner of SRRC columns. And the original cracks of RAC gradually were penetrated, leading to the spalling of partially RAC cover. With the continuous application of loads, RAC in the middle of specimens continued to crack and expanded outward, and the filamentous fracture of CFRP strips intensified. When the specimens reached the ultimate loads, CFRP strips in the middle of specimens was firstly broken with a loud sound, and large-scale spalling of partially RAC occurred. Meanwhile, the specimens had reached the ultimate failure state and the test was declared to be over. Figure 7 shows the failure characteristics and failure process of SRRC short columns confined by CFRP strips under axial compression loading.

According to the failure phenomenon of specimens, compared with the SRRC short columns fully wrapped with CFRP in Ref. [28], most of the CFRP strips are damaged in this test, and its utilization rate is high. Most of the columns fully wrapped with CFRP are damaged by fibers in the middle, which does not give full play to the performance of all CFRP. Therefore, CFRP strips wrapped SRRC columns has higher utilization rate.

3.2 Axial load-displacement curves

Figure 8 shows the axial load-displacement curves of SRRC short columns confined by CFRP strips with

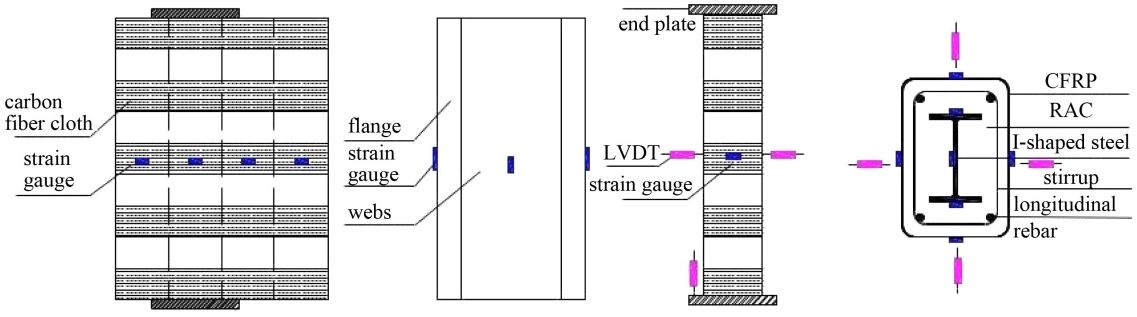

Fig. 6 Arrangement location of measuring points for the specimens.

different design parameters. It can be obtained from Fig. 8 that the columns confined by CFRP strips have the advantages of high bearing capacity and high stiffness under axial compression loading. Table 6 shows the main load characteristic values of SRRC short columns confined by CFRP strips. The effects of different parameters on the axial compression performance of the columns are as follows.

(1) It can be obtained from Fig. 8(a) and Table 6 that the replacement ratio of RCA has little impact on the initial stiffness of columns, and the initial stiffness of fully RAC column is slightly smaller than that of normal concrete column. The load-displacement curves of specimens gradually towards the horizontal ordinate with the increase of axial loads, showing that the stiffness of columns decreases. When the maximum load is about to be reached, the bearing capacity of specimens increases slowly. After the maximum load, the falling stage of the curves of specimens has a long platform and good deformation capacity. It is mainly because these columns are strongly restrained by CFRP strips, so that they still maintain good mechanical properties in the later stage of loading. In general, the axial bearing capacity of columns decreases slightly with the increase of substitution rate of RCA, and the bearing capacity of fully RAC column only decreases about 4.8% compared with ordinary concrete column. Obviously, the results show that the substitution percentage of RCA has little effect on the axial compression properties of columns, so the replacement rate of RCA in the columns can be taken as 100%.

(2) From Fig. 8(b) and Table 6, the spacing change of CFRP strips has a great influence on the axial stiffness of columns, and the initial stiffness gradually decreases with the increase of CFRP strips spacing. When the axial load increases to the maximum load, the bearing capacity of columns decreases obviously with the increase of CFRP strips spacing. For example, the bearing capacity of column with the CFRP strips spacing of 50 mm is 10.5% lower than that of the column with the CFRP strips spacing of 25 mm. After the peak load, with the reduction of CFRP strips spacing, the longer the descending section of load-displacement curves and the slower the downward trend. That is to say, the smaller the spacing of CFRP strips or the denser the CFRP strips and the better the restraint effect of CFRP strips, which is conducive to enhance the deformation capacity and bearing capacity of columns.

(3) Figure 8(c) is the influence of CFRP strips width on the load-displacement curves of columns. The axial force of each specimen is proportional to the displacement at the beginning of loading, and the constraint of CFRP strips on the specimens is small, which means that the strengthening effect of CFRP strips has not yet been exerted. The columns entered into the elastic-plastic stage with the increase of axial loads, and the relationship between force and displacement is approximately nonlinear. The axial bearing capacity and deformation of columns increase greatly with the increase of CFRP strips width, so it can be obtained that the width of CFRP strips has a significant influence on the properties of columns. For instance, the peak force of column with the CFRP strips width of 65 mm is 11.4% higher than that of the column with the CFRP strips width of 35 mm. In addition, the slope on the descending section of curves decreases with the increasing width of CFRP strips. It indicates that the increasing CFRP strips width is good for improving the deformation of SRRC columns.

(4) According to Fig. 8(d) and Table 6, the initial stiffness of the columns is improved with the increase of RAC strength. When the strength of RAC increases from C40 to C60, the peak load of column increases by about 23%. After the maximum load, the falling stage of load-displacement curve of specimen with the RAC strength of C50 or C60 becomes steeper than that of the specimen with the strength of C40. It indicates that the higher the RAC strength is, the higher the axial bearing capacity of columns, but the more obvious the brittleness of columns is. Therefore, for the RAC strength of C60 and above, it is suggested to mix the fiber in RAC or adopt the restraint measures outside the column to reduce its brittle failure as far as possible.

In addition, compared with the peak bearing capacity of short columns in literature [28], the bearing capacity of SRRC short columns wrapped with CFRP strips is about 6% lower than that fully wrapped with CFRP, indicating that the change from fully wrapped with CFRP to wrapped with CFRP strips has little impact on the mechanical properties of SRRC short columns.

Fig. 7 Failure characteristics and failure process of SRRC short columns by CFRP strips: (a) CFRP-SRRC-1; (b) CFRP-SRRC-2; (c) CFRP-SRRC-3; (d) CFRP-SRRC-4; (e) CFRP-SRRC-5; (f) CFRP-SRRC-6; (g) CFRP-SRRC-7; (h) CFRP-SRRC-8; (i) CFRP-SRRC-9.

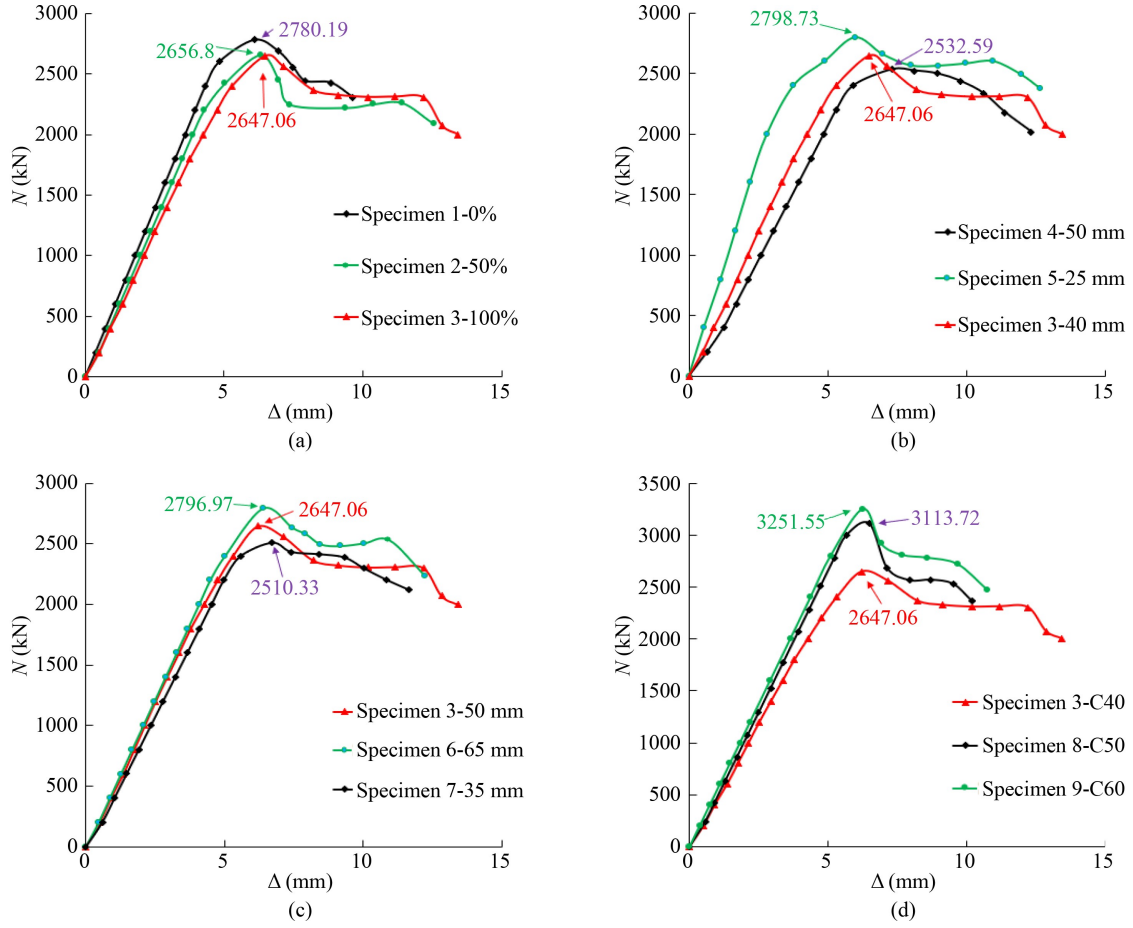

Fig. 8 Axial load-displacement curves of the specimens of short columns: (a) replacement rate of RCA; (b) CFRP strips spacing; (c) CFRP strips width; (d) RAC strength.

Table 6 Main load characteristic values of specimens

specimen number	cracking point		yield point		peak point		ultimate point	
	P_{cr} (kN)	Δ_{cr} (mm)	P_y (kN)	Δ_y (mm)	P_{max} (kN)	Δ_{max} (mm)	P_u (kN)	Δ_u (mm)
CFRP-SRRC-1	1390.10	2.48	1946.13	4.62	2780.19	6.10	2306.48	11.57
CFRP-SRRC-2	1328.40	2.53	1859.76	5.03	2656.80	6.31	2090.20	12.83
CFRP-SRRC-3	1323.53	2.73	1852.94	5.16	2647.06	6.49	2303.16	13.42
CFRP-SRRC-4	1519.78	4.42	2026.38	4.85	2532.59	7.30	2019.16	12.80
CFRP-SRRC-5	2099.05	2.93	2238.98	5.37	2798.73	5.98	2379.04	13.69
CFRP-SRRC-6	1538.33	3.03	2377.42	5.24	2796.97	6.38	2235.46	13.57
CFRP-SRRC-7	1380.68	2.95	2133.78	4.53	2510.33	6.72	2123.23	12.10
CFRP-SRRC-8	2023.92	3.89	2646.66	4.70	3113.72	6.47	2368.16	10.43
CFRP-SRRC-9	1950.93	3.52	2601.24	4.35	3251.55	6.26	2475.40	9.40

Note: P_{cr} is cracking load of point; Δ_{cr} is displacement of cracking point; P_y is load of yield point; Δ_y is displacement of yield point; P_{max} is load of peak point; Δ_{max} is displacement of peak point; P_u is load of ultimate point; Δ_u is displacement of ultimate point.

3.3 Strain characteristics of columns confined by carbon fiber reinforced plastics strips

3.3.1 Strain of profile steel and rebars

The axial load-strain relationship of profile steel and rebars in the short columns under axial compression loading is described in Fig. 9, where "M, F, Y" in "M-F-1" and "M-Y-1" represent the middle position of specimens, web and flanges of profile steel, respectively. At the beginning of loading, the strain values of profile steel and rebars in the specimens are very small, and their strain changes linearly with the axial loads. When about 70% of maximum load is reached, the profile steel flange

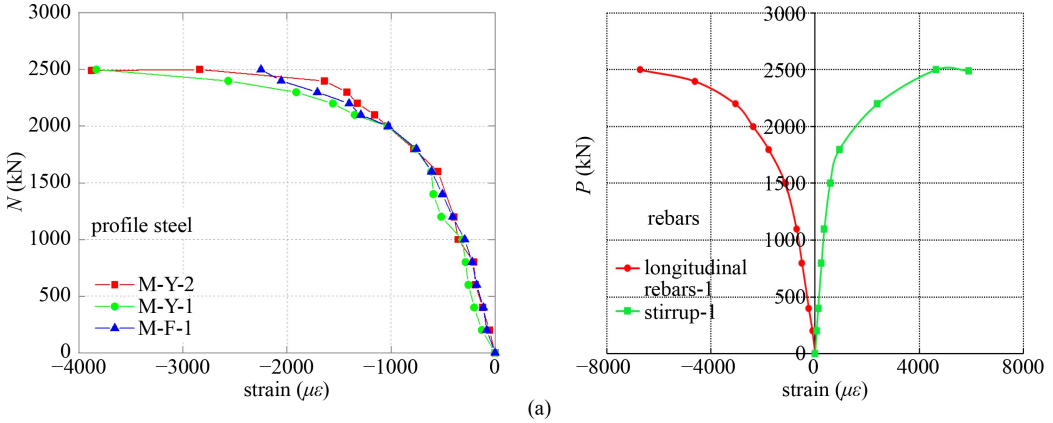
N (kN)
profile steel
M-Y-2
M-Y-1
M-F-1
strain (με)
P (kN)
rebars
longitudinal rebars-1
stirrup-1
strain (με)

(a)

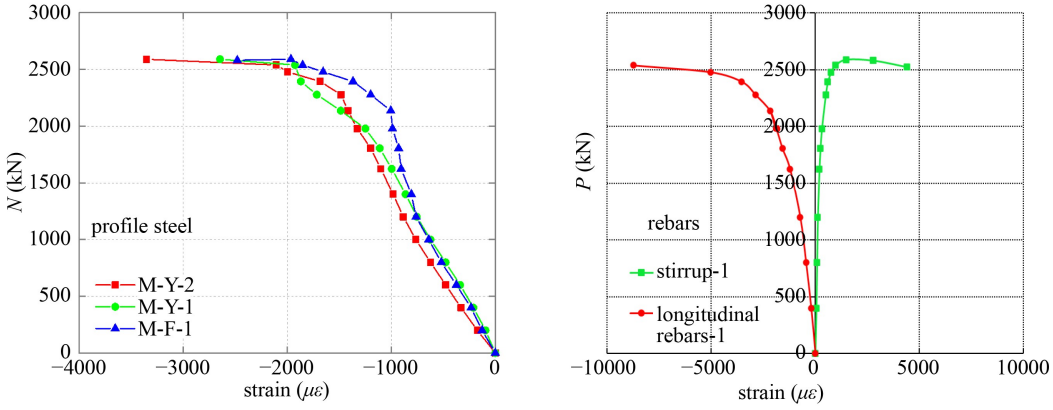
N (kN)
profile steel
M-Y-2
M-Y-1
M-F-1
strain (με)
P (kN)
rebars
stirrup-1
longitudinal rebars-1
strain (με)

(b)

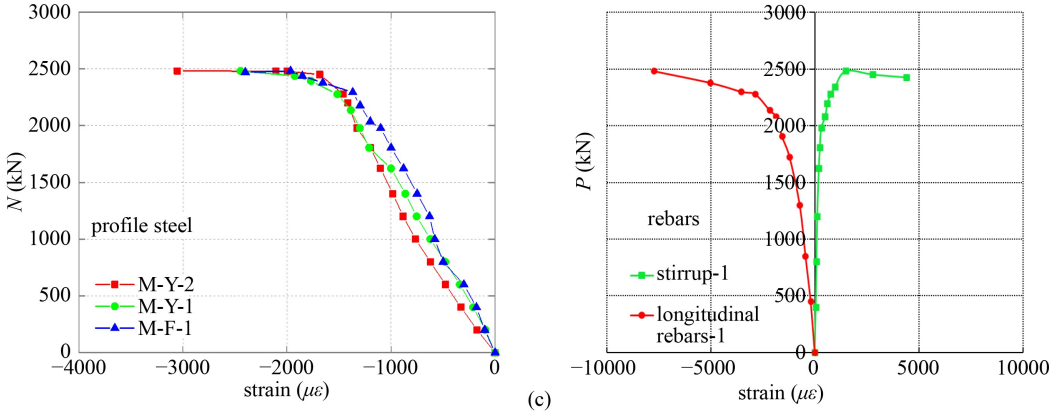
N (kN)
profile steel
M-Y-2
M-Y-1
M-F-1
strain (με)
P (kN)
rebars
stirrup-1
longitudinal rebars-1
strain (με)

(c)

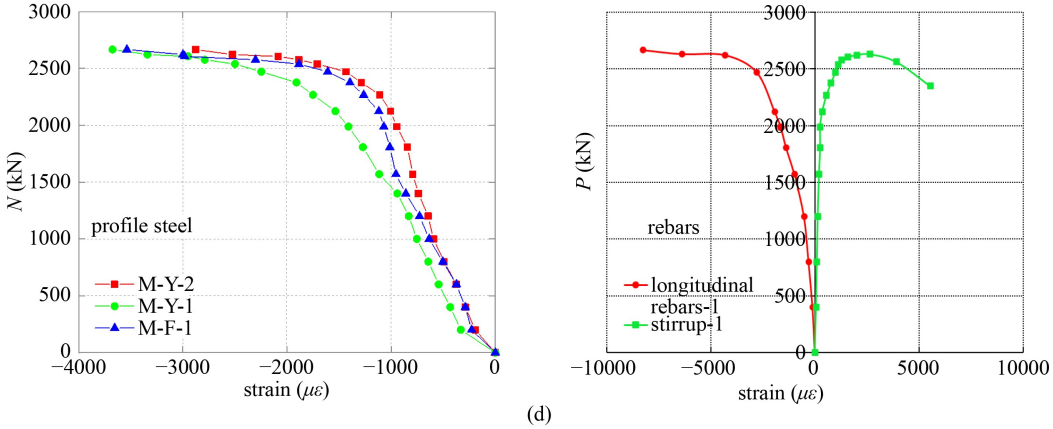
N (kN)
profile steel
M-Y-2
M-Y-1
M-F-1
strain (με)
P (kN)
rebars
longitudinal rebars-1
stirrup-1
strain (με)

(d)

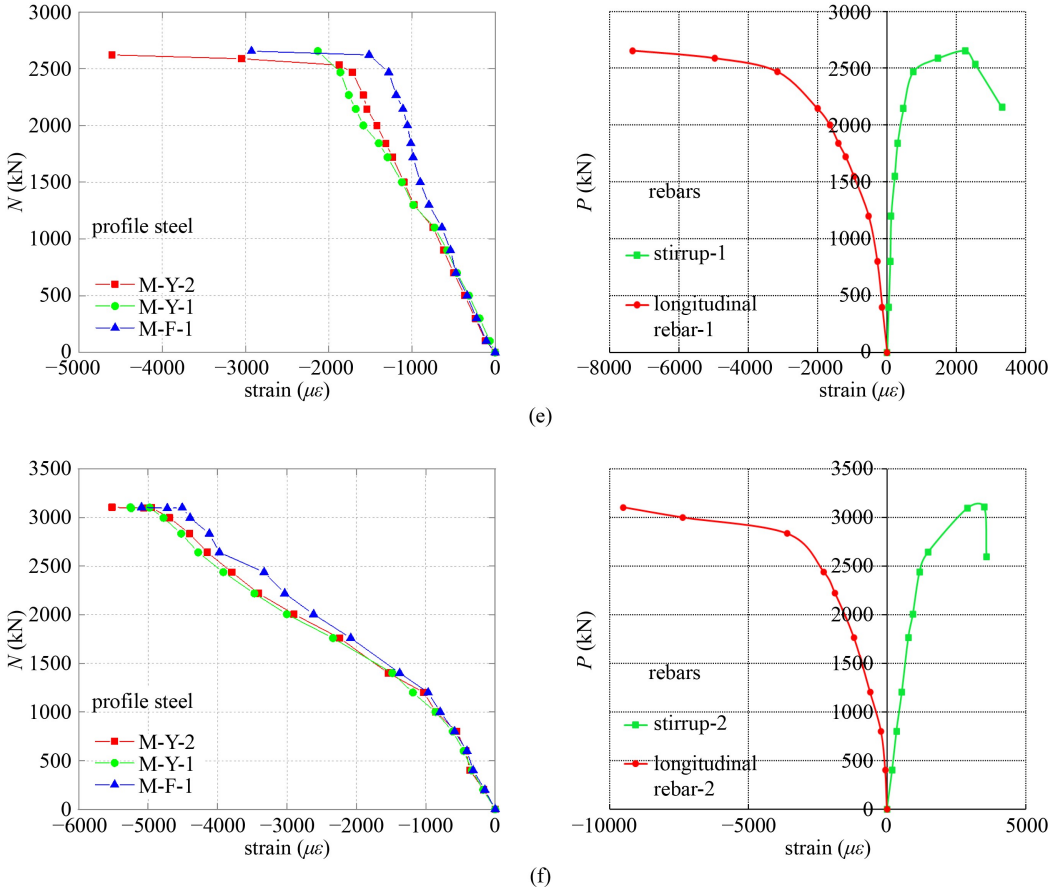

Fig. 9 Axial load-strain curves of profile steel and rebars in the typical specimens: (a) CFRP-SRRC-2; (b) CFRP-SRRC-3; (c) CFRP-SRRC-4; (d) CFRP-SRRC-5; (e) CFRP-SRRC-6; (f) CFRP-SRRC-8.

begins to yield and its strain is about 1400$\mu\varepsilon$. And when about 80% of maximum load is reached, the profile steel web also reaches the yield state, and its strain value is about 1900$\mu\varepsilon$. After maximum load, the strain growth rate of profile steel accelerates until it yields completely, and then longitudinal rebars and stirrups also reach the yield state one after another. At this moment, the strain values of longitudinal rebars and stirrups are about 2200$\mu\varepsilon$ and 2000$\mu\varepsilon$, respectively. From the strain change comparison between profile steel and rebars, it can be seen that the strain of profile steel is significantly greater than that of rebars under the same axial force, and the growth rate is also faster than that of rebars. That is to say, the profile steel in the columns first reaches the yield state under the axial compression loading, then the longitudinal rebars yields. In addition, comparing Figs. 9(a) and 9(b), it can be concluded that the initial strain of profile steel increases rapidly with the increase of RCA replacement rate r. However, the strain growth rate of profile steel with r = 100% slows down with the increase of load, which also causes it to yield later than the profile steel with r = 50%. Similarly, the yield of rebars slows down with the increase of RCA substitution rate. In comparison Figs. 9(b)–9(d), the spacing of CFRP strips has little effect on the initial strain of profile steel and rebars. With the increase of strip spacing, the profile steel and rebars yield earlier. Comparing Figs. 9(b) and 9(e), the wider the CFRP strip, the later the profile steel and rebars enter the yield time. As can be obtained from Figs. 9(b) and 9(f), the higher the RAC strength level, the faster the strain growth rate of profile steel and the easier it is to yield.

3.3.2 Strain characteristics of recycled aggregate concrete

The axial load-strain curves of RAC in SRRC columns confined by CFRP strips are shown in Fig. 10. It can be obtained from Fig. 10 that at the beginning of loading, the trend of load-strain curves of all the columns is basically the same, and the strain of RAC varies linearly with the load. Fig. 10(a) is the strain change of RAC in the columns under different replacement rate of RCA. When the load increases to 1700 kN, the strain value of RAC is about 1900$\mu\varepsilon$, and the strain value of RAC increases nonlinearly with the axial force. When the load increases to 80% and 100% of peak load, the strain values of RAC are about 2400$\mu\varepsilon$ and 5000$\mu\varepsilon$, respectively. Under peak loads, the strain value of RAC with the replacement rate of RCA for 100% increases by 46.8% compared with ordinary concrete column. Obviously, it shows that the

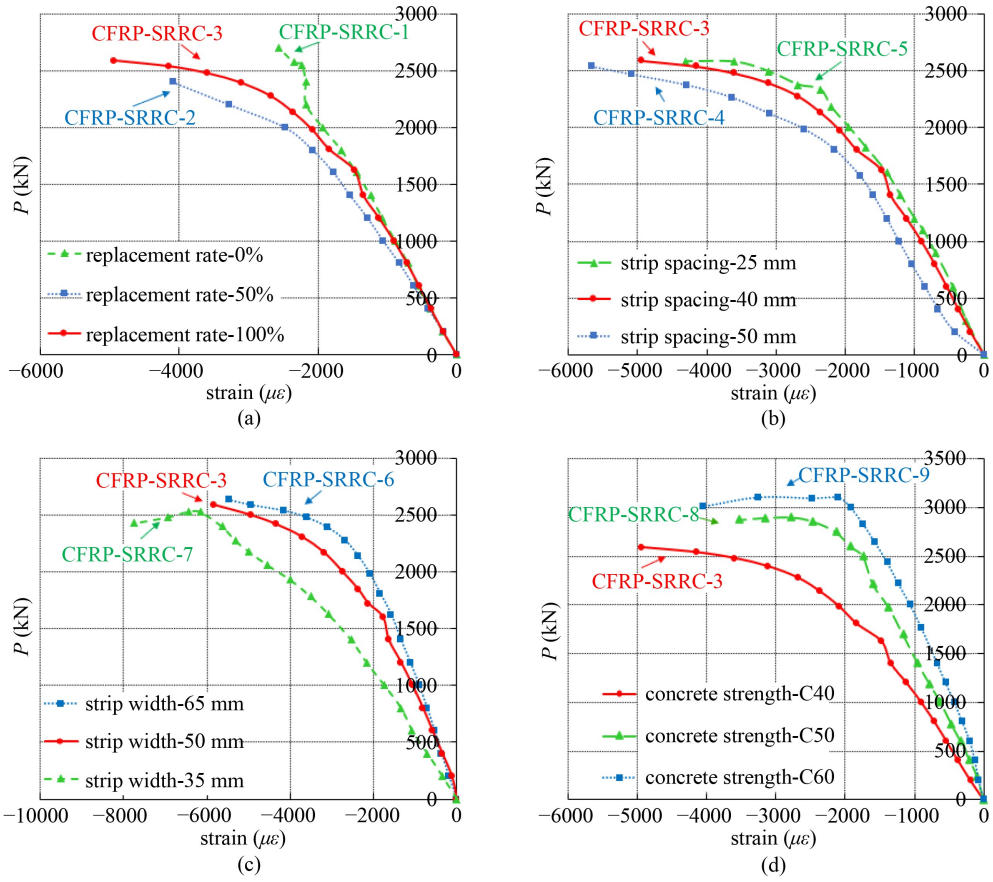

Fig. 10 Axial load-strain relationship of RAC in the specimens: (a) replacement rate of RCA; (b) CFRP strips spacing; (c) CFRP strips width; (d) RAC strength.

strain value of RAC increases obviously with the increasing substitution rate of RCA. From Figs. 10(b) and 10(c), the wider the CFRP strips width or the smaller the CFRP strips spacing, the lower the strain values of RAC, which indicates that the width and spacing of CFRP strips have a significant impact on the deformation of RAC. From Fig. 10(d), the strain values of RAC with the strength of C40, C50 and C60 are about 4900$\mu\varepsilon$, 3455$\mu\varepsilon$ and 2094$\mu\varepsilon$, respectively. The strain value of RAC with the strength of C50 is 29.5% lower than that of RAC with the strength of C40, and the strain value of RAC with the strength grade of C60 is 39.4% lower than that of RAC with the strength grade of C50. It indicates that the higher the strength of RAC, the worse the deformation capacity of columns.

3.3.3 Strain of carbon fiber reinforced plastics strips

The circumferential strain of CFRP strips was measured by pasting the strain gauges on the surface of CFRP strips in the columns, so as to obtain the strain rule of CFRP strips under of axial compression loading. Figure 11 shows the axial load-strain relationship of CFRP strips in the columns. At the initial stage of loading, the strain values of CFRP strips increase slowly, and the axial force and strain of CFRP strips change almost linearly. After the cracking of RAC, the strain values of CFRP strips begin to increase rapidly. When it reaches about 80% of peak load, the strain values of CFRP strips increase nonlinearly with the force, and the strain values of CFRP strips are about 1400$\mu\varepsilon$. When maximum load is reached, the strain values of CFRP strips are about 2000$\mu\varepsilon$. At this stress stage, RAC in the columns cracks seriously and its volume expansion is also obvious, which causes to a rapid increase in the strain of CFRP strips. When the CFRP strips of columns are broken, the maximum strain of CFRP strips can reach about 13000$\mu\varepsilon$ (i.e., CFRP-SRRC-5 specimen). Meanwhile, the strain values of the CFRP strips with the width of 65 mm and 35 mm reach 10200$\mu\varepsilon$ and 6777$\mu\varepsilon$, respectively. Compared to the CFRP strips with the width of 65 mm, the strain value of CFRP strips with the width of 35 mm is reduced by about 33.5%. Besides, compared to the CFRP strips with the spacing of 50 mm, the strain value of CFRP strips with the spacing of 25 mm is increased by 60.9%. The results clearly show that the wider the CFRP strips width or the smaller the CFRP strips spacing, the stronger the restraint effect of CFRP strips on the SRRC columns.

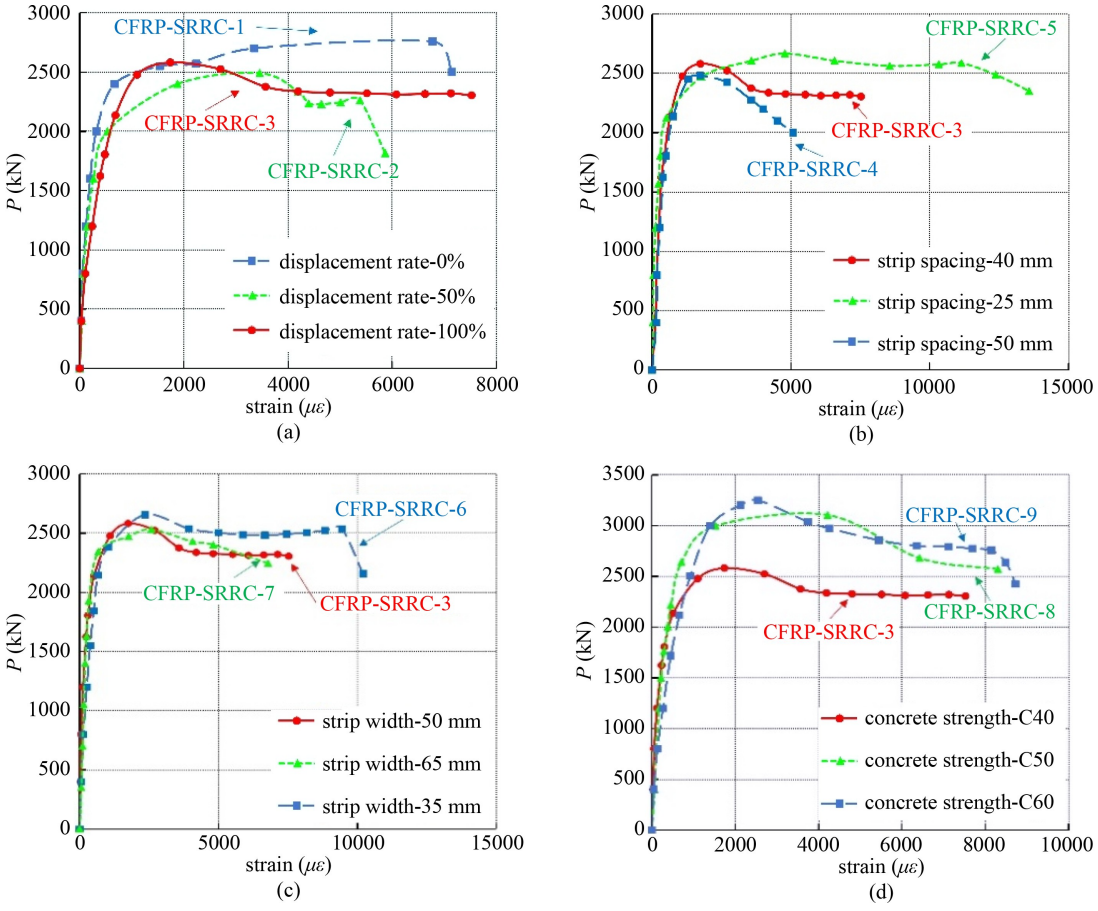

Fig. 11 Axial load-strain curves of CFRP strips in the specimens: (a) replacement rate of RCA; (b) CFRP strips spacing; (c) CFRP strips width; (d) RAC strength.

4 Finite element analysis of SRRC columns confined by carbon fiber reinforced plastics strips

4.1 Constitutive relationship of materials in the columns

4.1.1 Constitutive model of recycled aggregate concrete

(1) Compression constitutive model of RAC

The reasonable constitutive model can well reflect the mechanical properties of materials, which is very important for the finite element calculation of structures or components. The compression constitutive model of RAC in this research is based on the compressive stress-strain curve of RAC proposed by Xiao [29]. Its equation can be expressed as follows:

$$y = \begin{cases} ax + (3-2a)x^2 + (a-2)x^3, & 0 \leqslant x < 1, \\ \dfrac{x}{b(x-1)^2 + x}, & x \geqslant 1, \end{cases} \tag{1}$$

where $x = \varepsilon/\varepsilon_0$, $y = \sigma/f_c$; ε_0 is the maximum compressive strain of RAC; f_c is the uniaxial compressive strength of RAC. The f_c values of RAC with strength of C40, C50, and C60 are 32.5, 40, and 46 MPa, respectively; the experimental research show that the replacement percentage of RCA has a certain effect on the mechanical performance of RAC, so the effect of substitution rate of RCA should be considered in the compression constitutive model of RAC. With the increasing substitution percentage of RCA, the peak strain of RAC increases gradually, so the effect of substitution rate r on the peak strain ε_0 of RAC needs to be considered, which can be calculated according to the calculation method proposed by Xiao [29], as shown in Eq. (2). In addition, the rise and fall sections on the constitutive curves of RAC are also different from the ordinary concrete, which can be adjusted by parameters a and b. The expressions of parameters a and b in Eq. (1) are shown in Eq. (3).

$$\begin{cases} \varepsilon_0 = \{0.00076 + [(0.626 f_c - 4.33) \times 10^{-7}]^{0.5}\} \times \left[1 - \dfrac{r}{B(r)}\right], \\ B(r) = 65.715r^2 - 109.43r + 48.989, \end{cases} \tag{2}$$

$$\begin{cases} a = 2.2 \times (0.748r^2 - 1.231r + 0.975), \\ b = 0.8 \times (7.6483r + 1.142). \end{cases} \tag{3}$$

(2) Tension constitutive model of RAC

In this research, the rising stage and falling stage of tensile stress-strain curve of RAC were determined according to literatures [30–31], and the influence of substitution percentage of RCA on the tensile properties of RCA is also considered in the tension constitutive model. The peak tensile strain and tensile stress of RAC with the strength grades of C40, C50, and C60 under three substitution rates can be calculated based on Eq. (5), and then brought into Eq. (4) to obtain the tensile constitutive relationship of RAC.

$$\begin{cases} y = 1.2x - 0.2x^6, & x \leqslant 1, \\ y = \dfrac{x}{\alpha_t (x-1)^{1.7} + x}, & x > 1, \\ y = \dfrac{\sigma}{f_t}, \\ x = \dfrac{\varepsilon}{\varepsilon_t}, \end{cases} \tag{4}$$

$$\begin{cases} f_t = (cr + 0.24)(f_{cu})^{\frac{2}{3}}, \\ \varepsilon_t = (55 + dr)(f_t)^{0.54} \times 10^{-6}, \end{cases} \tag{5}$$

where α_t is the parameter values on the descending section of tensile stress-strain curve of RAC, which is determined according to Table 7; f_t is the maximum tensile stress of RAC; f_{cu} is the cube compressive strength of RAC; ε_t is the maximum tensile strain of RAC, calculated on the basis of formula (5); In addition, the parameters c and d in Eq. (5) can be –0.06 and 14, respectively.

Based on the existing experimental research, the compression and tensile damage of RAC is the same as that of normal concrete. Because of the lack of plastic damage of RAC, in order to facilitate the calculation, so the damage model of ordinary concrete was adopted by adjusting input parameters in this paper. In ABAQUS software, the plastic damage of concrete material can not only consider the biaxial ratio, but also consider the interaction of biaxial tensile and compressive properties of concrete material, which well reflects the actual stress situation of concrete material. The plastic damage model includes two failure modes of concrete material, namely compressive failure and tensile cracking. In this research, the damage criterion of RAC is determined by controlling the equivalent stress on the yield surface of RAC. When RAC are damaged, the material will enter the softening stage of stress-strain curve. The main parameters of concrete damaged plasticity are as follows: the eccentricity $\varepsilon = 0.1$; the invariant stress ratio $K_c = 0.6667$; the dilation angle $\psi = 30°$; the ultimate strength rate of the biaxial compression and the uniaxial compression $f_{bo}/f_{co} = 1.16$ and the viscosity parameter $\mu = 0.0005$. The yield conditions of RAC are shown in Fig. 12, and Fig. 13 shows a typical yield surface on the off plane of RAC.

Table 7 Parameter values on the uniaxial tensile stress-strain curve α_t of RAC

f_t (N/mm^2)	ε_t (10^{-6})	α_t
1.0	65	0.31
1.5	81	0.70
2.0	95	1.25
2.5	107	1.95
3.0	118	2.81
3.5	128	3.82
4.0	137	5.00

4.1.2 Constitutive model of profile steel and rebars

The constitutive model of profile steel and rebars adopted simplified stress-strain curve in the numerical model, which is characterized by two plastic platforms, as shown in Eq. (6). The constitutive model can consider the strengthening stage of steel directly after yield, and the strength of steel remains unchanged in the plastic flow stage. In a word, the model accords with the material characteristics, considers the strengthening effect of steel, and better reflects the mechanical process of steel.

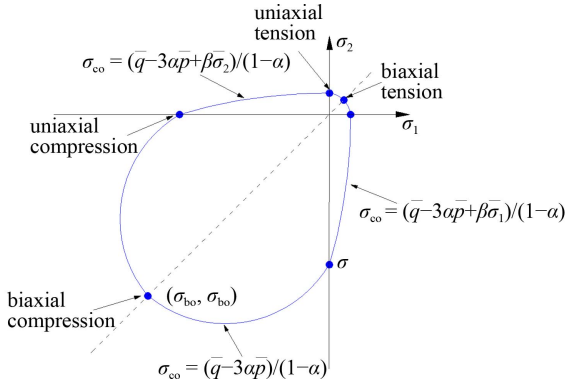

Fig. 12 Yield surface of RAC under the plane stress.

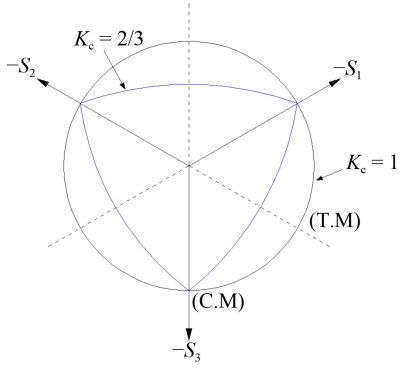

Fig. 13 Yield surface of RAC determined by different K_c values in the deviatoric plane.

$$\sigma=\begin{cases}E_s\varepsilon, & \varepsilon<\varepsilon_y,\\ f_y, & \varepsilon_y\leqslant\varepsilon<k_1\varepsilon_y,\\ k_3f_y+\dfrac{E_s(1-k_3)}{\varepsilon_y(k_2-k_1)^2}(\varepsilon-k_2\varepsilon_y)^2, & k_1\varepsilon_y\leqslant\varepsilon<k_2\varepsilon_y,\\ f_u, & \varepsilon\geqslant k_2\varepsilon_y,\end{cases} \tag{6}$$

where f_y is the yield stress; ε_y is the yield strain; E_s is the elastic modulus; k_1, k_2, and k_3 are the control parameters of curve shape, respectively, which can be taken as k_1 = 4.5, k_2 = 45, and k_3 = 1.4.

In this study, the failure criterion of steel conforms to the Mises yield criterion, as shown in Eq. (7). It is usually considered that as follows: on the one hand, the steel is in an elastic state before yielding and the relationship of stress−strain is linear; on the other hand, under certain deformation conditions, when the elastic energy of the change of shape per unit volume of material reaches a constant, the steel material will yield and enter the plastic state.

$$\sigma_s=\sqrt{1/2[(\sigma_1-\sigma_2)^2+(\sigma_2-\sigma_3)^2+(\sigma_1-\sigma_3)^2]}, \tag{7}$$

where σ_1, σ_2, and σ_3 are the first, second and third principal stresses of steel, respectively, and σ_s is the yield strength of steel.

4.1.3 Constitutive model of carbon fiber reinforced plastics strips

As a composite material, CFRP is considered as an elastic material, and its failure basically meets the Hashin criterion. The progressive damage theory based on the energy method is adopted in the finite element simulation. It is considered that the material will not be broken immediately after damage, but the material performance will degrade, and more loads will be borne through the surrounding undamaged elements. With the continuous decline of the bearing capacity of the surrounding material elements, the undamaged elements will gradually decrease, and the material will not be broken until the damage exceeds the specified value. Material damage is divided into: the fiber direction tensile failure, the fiber direction compression failure, the tensile failure in vertical fiber direction, the vertical fiber compression failure. Material damage is determined by the following formula.

Fiber direction tensile failure:

$$F_{ft}=\left(\frac{\hat{\sigma}_{11}}{X^T}\right)^2+\alpha\left(\frac{\hat{\sigma}_{12}}{S^L}\right)^2=1,\qquad(\hat{\sigma}_{11}\geqslant 0). \tag{8}$$

Fiber direction compression failure:

$$F_{tc}=\left(\frac{\hat{\sigma}_{11}}{X^C}\right)^2=1,\qquad(\hat{\sigma}_{11}\leqslant 0). \tag{9}$$

Tensile failure in vertical fiber direction:

$$F_{mt}=\left(\frac{\hat{\sigma}_{22}}{Y^T}\right)^2+\left(\frac{\hat{\sigma}_{12}}{S^L}\right)^2=1,\qquad(\hat{\sigma}_{22}\geqslant 0). \tag{10}$$

Vertical fiber compression failure:

$$F_{mc}=\left(\frac{\hat{\sigma}_{22}}{2S^T}\right)^2+\left[\left(\frac{Y^C}{2S^T}\right)^2-1\right]\frac{\hat{\sigma}_{22}}{Y^C}+\left(\frac{\hat{\sigma}_{12}}{S^L}\right)^2=1,\qquad(\hat{\sigma}_{22}\leqslant 0). \tag{11}$$

The above formulas are used to judge the damage initiation of the material. When the value of F reaches 1.0, it means that the material damage begins at this time, and when F is less than 1.0, it means that the material is not damaged. The six strength values in the above formulas are actually related to the material damage, it can be described as follows: the longitudinal compressive strength X^C = 1200 MPa, the longitudinal tensile strength X^T = 3565.2 MPa, the transverse compressive strength Y^C = 190 MPa, the transverse tensile strength Y^T = 62 MPa, the longitudinal shear strength S^L = 81 MPa, the transverse shear strength S^T = 81 MPa. It is incomplete to use the above four formulas for the failure analysis of CFRP material, because it can only predict the beginning of damage and lacks the stiffness degradation after damage. Therefore, Hashin [32] also puts forward the damage evolution based on energy, that is, the energy required for the complete fracture of the material along the interface. The fracture energy corresponding to the four failure modes of CFRP material input in this paper is: the longitudinal compressive fracture energy G_{fcc} = 75 N/mm, the longitudinal tensile fracture energy G_{ftc} = 50 N/mm, the transverse tensile fracture energy G_{mtc} = 0.25 N/mm as well as the transverse compressive fracture energy G_{mcc} = 0.75 N/mm. The fracture energy is taken as the specified value of failure, which is used to judge whether the material is completely broken.

4.2 Contact settings between materials

During the establishment of numerical model, profile steel and RAC were defined as the contact attributes, and the bond slip between steel and concrete is considered. The relationship between the critical tangential stress τ_{crit} and the normal stress p conforms to Eq. (12), and the friction coefficient μ can be taken as 0.6. In addition, CFRP and RAC were defined as the binding relationship between surfaces, and the rebars were built into RAC. The top and bottom of SRRC short column were respectively coupled at two points. The bottom of column was fixed and constrained to limit movement and rotation. The coupling point was established above the column, and the axial force was applied to the column top in the form of uniform load through the coupling point, so as to avoid local damage to the column top.

$$\tau_{\text{crit}} = \mu p \geqslant \tau_{\text{bond}}. \quad (12)$$

The mesh density directly affects the correctness and efficiency on the numerical simulation of column. Too large mesh will lead to very low calculation accuracy of the model, but too small mesh may lead to non-convergence and reduce the calculation speed. In order to increase the calculation accuracy, the grid at the corner of column was densified. The solid parts such as RAC and profile steel were divided into hexahedral calculation elements (C3D8R), and CFRP was divided into quadrilateral shell elements (S4R), as well as the rebars were divided into two node line elements (T3D2). The mesh division on the numerical model of columns is shown in Fig. 14.

4.3 Results of finite element analysis

4.3.1 Stress nephogram characteristics

Through the calculation of numerical model, the stress nephogram and mechanical properties indexes of SRRC short columns confined by CFRP strips can be obtained, as described in Figs. 15–18. At the initial stage of loading, the columns were in an elastic state and the stress of various materials was very small. The stress of specimens increased with the increase of loads, but its deformation was not obvious. After the cracking of RAC, the specimens gradually deformed obviously with the increase of force, and the middle area of columns was slightly bulging. When increasing to 80% of peak load, the stress of profile steel reached the yield strength, and the stress in the middle of steel web and steel flange exceeded 235 MPa. Meanwhile, although the stress of rebars, RAC and CFRP strips increased with the increase of force, they still had not the yield strength. When the peak load was reached, the stress of profile steel continued to increase and the yield area of profile steel gradually expanded. At this stage, the stress in the middle of longitudinal rebars exceeded 360 MPa and they had yielded, but the stirrups did not enter the yield state. The tensile stress of RAC at the corner of columns far exceeded 2.4 MPa, which shows the cracking of RAC at the corner of columns was serious. By the way, although the CFRP strips had not yet reached the yield strength, their expansion deformation was more obvious because of the cracking of RAC. When the loading ended, the stress of RAC exceeded 36 MPa, which shows that RAC was seriously damaged under the compression stress. While profile steel and rebars in the columns almost completely yielded. In addition, the stress of CFRP strips in the middle of columns reached 3216 MPa, which was close to the ultimate tensile strength, and the ultimate failure was mainly due to the fracture of CFRP strips.

As a whole, the failure characteristics of the columns indicate that the profile steel first yields, then the longitudinal rebars yields, and RAC is crushed, finally the CFRP strips are broken. Because of the good strengthening effect of CFRP strips, the columns have high bearing capacity and stiffness. In addition, when these columns are damaged, they do not show obvious brittleness and still have a certain deformation capacity.

4.3.2 Load-displacement calculated curves

Table 8 lists the comparison results of main load characteristic values of specimens under different test design parameters. The comparisons of load-displacement

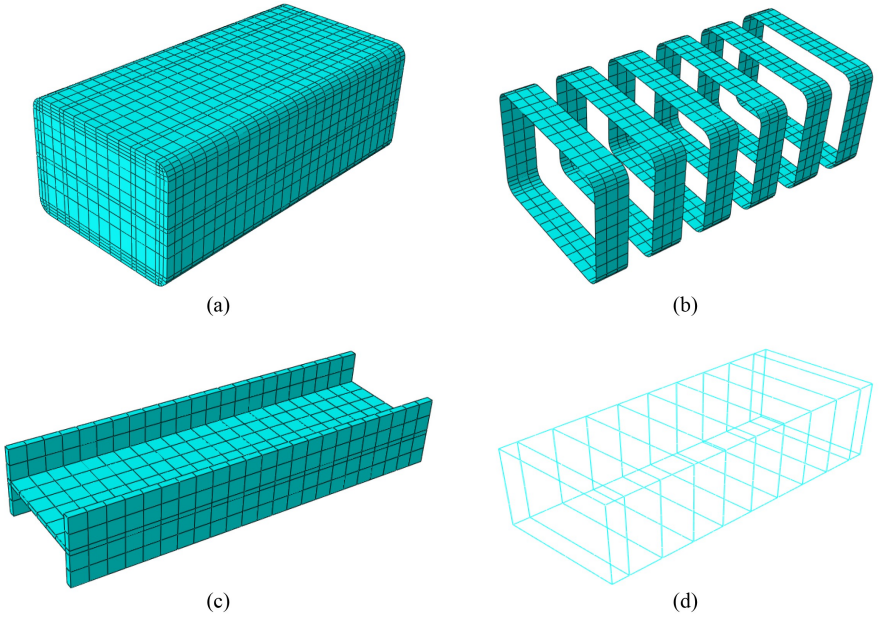

Fig. 14 Mesh division of SRRC short columns confined by CFRP strips: (a) RAC; (b) CFRP strips; (c) profile steel; (d) rebars.

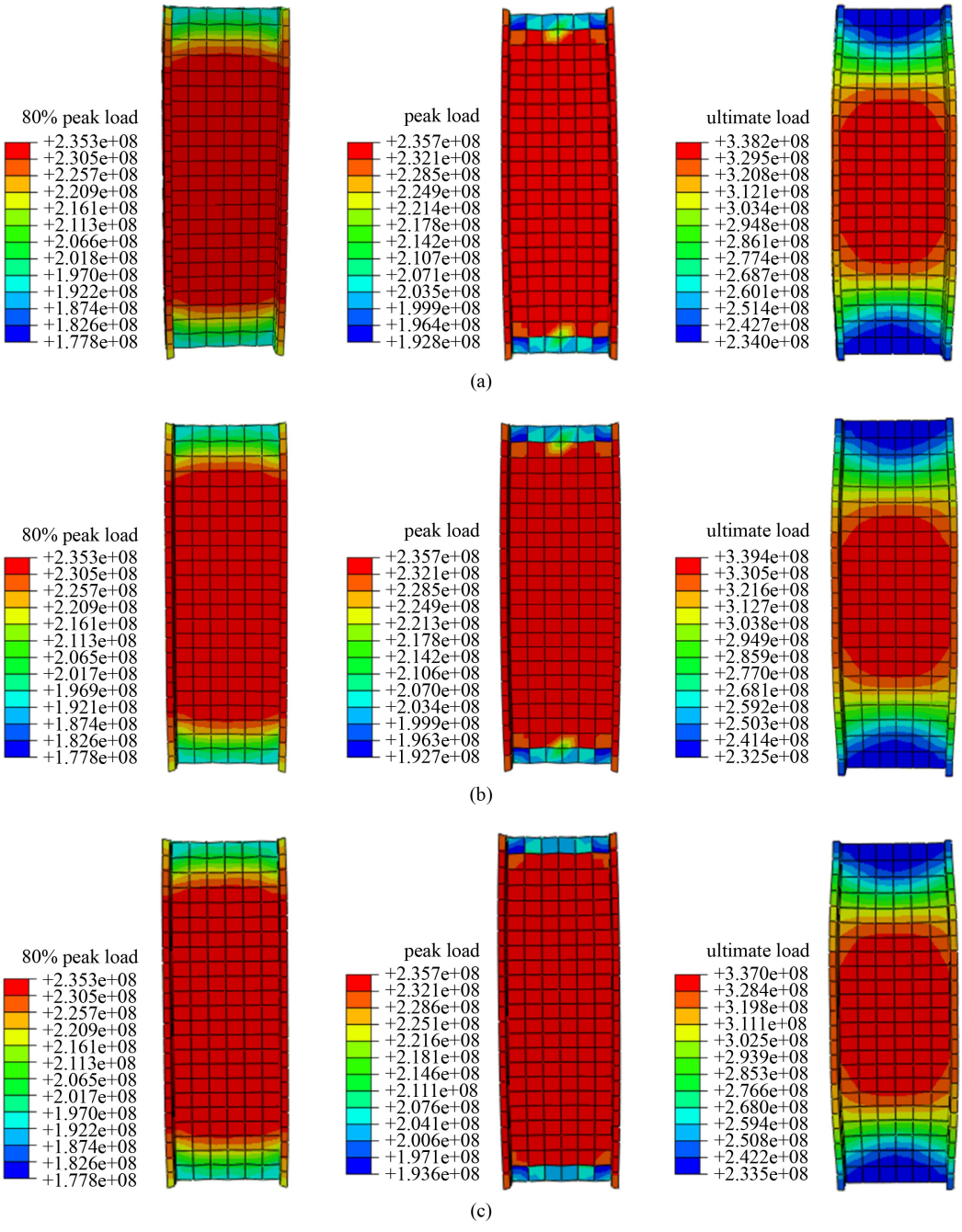

Fig. 15 von−Mises stress nephogram of profile steel in the typical specimens: (a) stress nephogram of profile steel in the specimen of CFRP-SRRC-3; (b) stress nephogram of profile steel in the specimen of CFRP-SRRC-4; (c) stress nephogram of profile steel in the specimen of CFRP-SRRC-7.

curves of specimens between the test investigation and numerical simulation are shown in Fig. 19. It can be obtained from Fig. 19 that the test and calculation load-displacement curves of columns are basically consistent before reaching peak loads, and the slopes of both curves are almost the same. However, when peak load is reached, the simulated values on the axial bearing capacity of specimens are certain different from the test values. According to Table 8, the maximal relative error of peak load between the experimental value and simulated value of column is 13.67% (i.e., CFRP-SRRC-8). After the peak load, the falling stage of the curves first decreases rapidly, and then tends to decrease slowly, which shows that the specimen shows good deformation ability in the later stage of loading. By the way, although there is a certain difference between the test curves and numerical curves in the descending section, the descending stage of curves has the same trend. To sum up, because the columns are restrained by CFRP strips, the bearing capacity will not drop rapidly to the end, so as

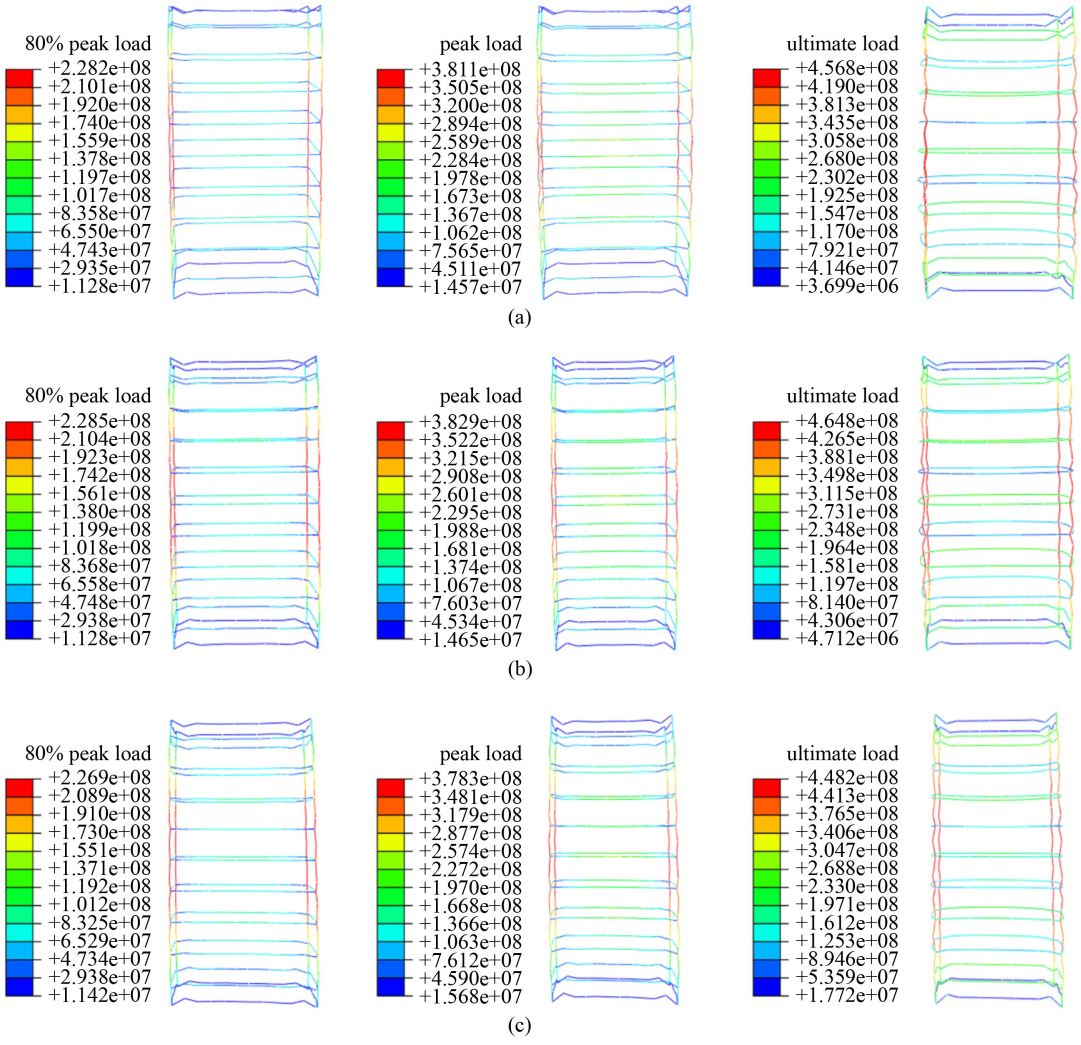

Fig. 16 von−Mises stress nephogram of rebars in the typical specimens: (a) stress nephogram of rebars in the specimen of CFRP-SRRC-3; (b) stress nephogram of rebars in the specimen of CFRP-SRRC-4; (c) stress nephogram of rebars in the specimen of CFRP-SRRC-7.

to slow down the decline of bearing capacity until CFRP strips are broken. The above analysis results show that the columns have high deformation capacity and bearing capacity under the constraint of CFRP strips.

4.4 Parameter analysis of the columns confined by carbon fiber reinforced plastics strips

Through the above comparison of test and simulation of columns, there is little difference between experiment and simulation. From the above simulation results, it can be seen that this model can be suitable for the simulation of this kind of columns. Based on this numerical calculation, the parameter analysis of SRRC short columns confined by CFRP strips was put into effect in this study. The influence of extended parameters such as the profile steel strength, chamfer radius of cross-section, CFRP strips width and CFRP strips layers on the axial compression properties of columns were mainly considered, as shown in Table 9. The geometric dimension of simulated columns was the same as that of test specimens, and the replacement rate of RCA and CFRP strips spacing were 100% and 40 mm respectively in all simulated columns. Figure 20 displays load-displacement curves of the columns under different parameters. The effect characteristics of extended parameters on the axial compression properties of columns are as follows.

(1) It can be obtained from Fig. 20(a) that the profile steel strength has a great impact on the axial bearing capacity of columns. The axial bearing capacity is greatly improved with the increase of steel strength, and the bearing capacity increases by about 18.9% with the increase of steel strength from Q235 to Q390. At the beginning of loading, the columns are in the elastic state and the force is proportional to the displacement. The initial stiffness of columns is basically the same under different steel strength. When 70% of peak load is reached, the slope of curves gradually decreases, which means that the columns enter the nonlinear state. There are obvious differences in the curves of columns under

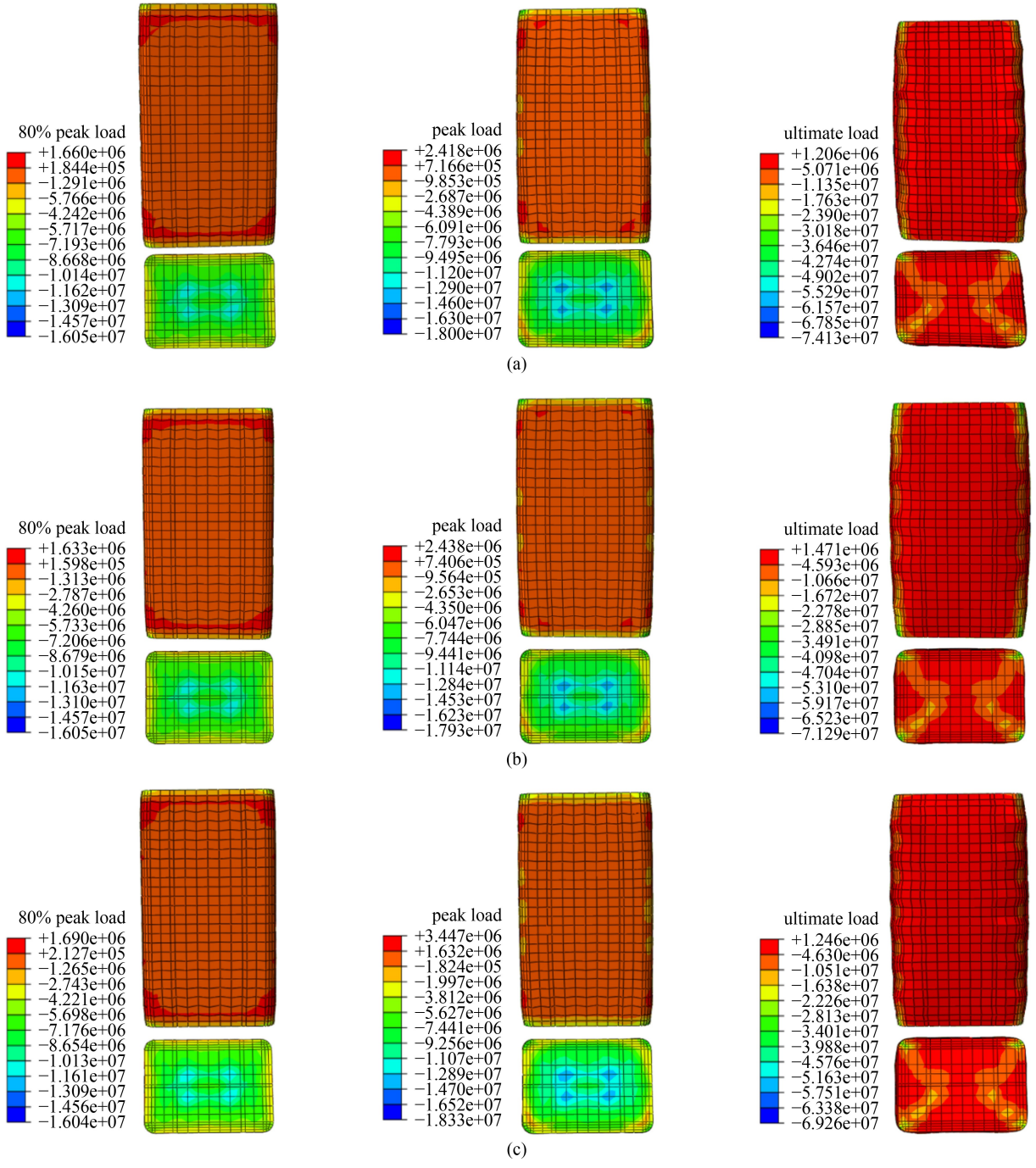

Fig. 17 Maximum principal stress nephogram of RAC in the typical specimens: (a) stress nephogram of RAC in the specimen of CFRP-SRRC-3; (b) stress nephogram of RAC in the specimen of CFRP-SRRC-4; (c) stress nephogram of RAC in CFRP-SRRC-7 specimen.

different steel strength. The higher the strength of profile steel, the growth rate of bearing capacity of column is significantly greater than that of column with a low strength of profile steel. The descending stage of curves shows the characteristics of first fast and then slow in the later stage of loading, indicating that the columns have a good deformation capacity.

(2) It can be obtained from Fig. 20(b) that the impact of CFRP strips width on the load-displacement curves of columns. According to Fig. 20(b), the narrower the CFRP strips width, the faster the curve slope of columns changes. When the CFRP strips becomes wider, the axial bearing capacity of columns also enhances. The CFRP strips with a width less than 20 mm have little enhancement influence on the bearing capacity of columns, while the restraint effect is better when the CFRP strip width is greater than 30 mm. Compared with the column without the restraint effect of CFRP strips, the bearing capacity of it can be increased by 15% with the CFRP strip width of 65 mm.

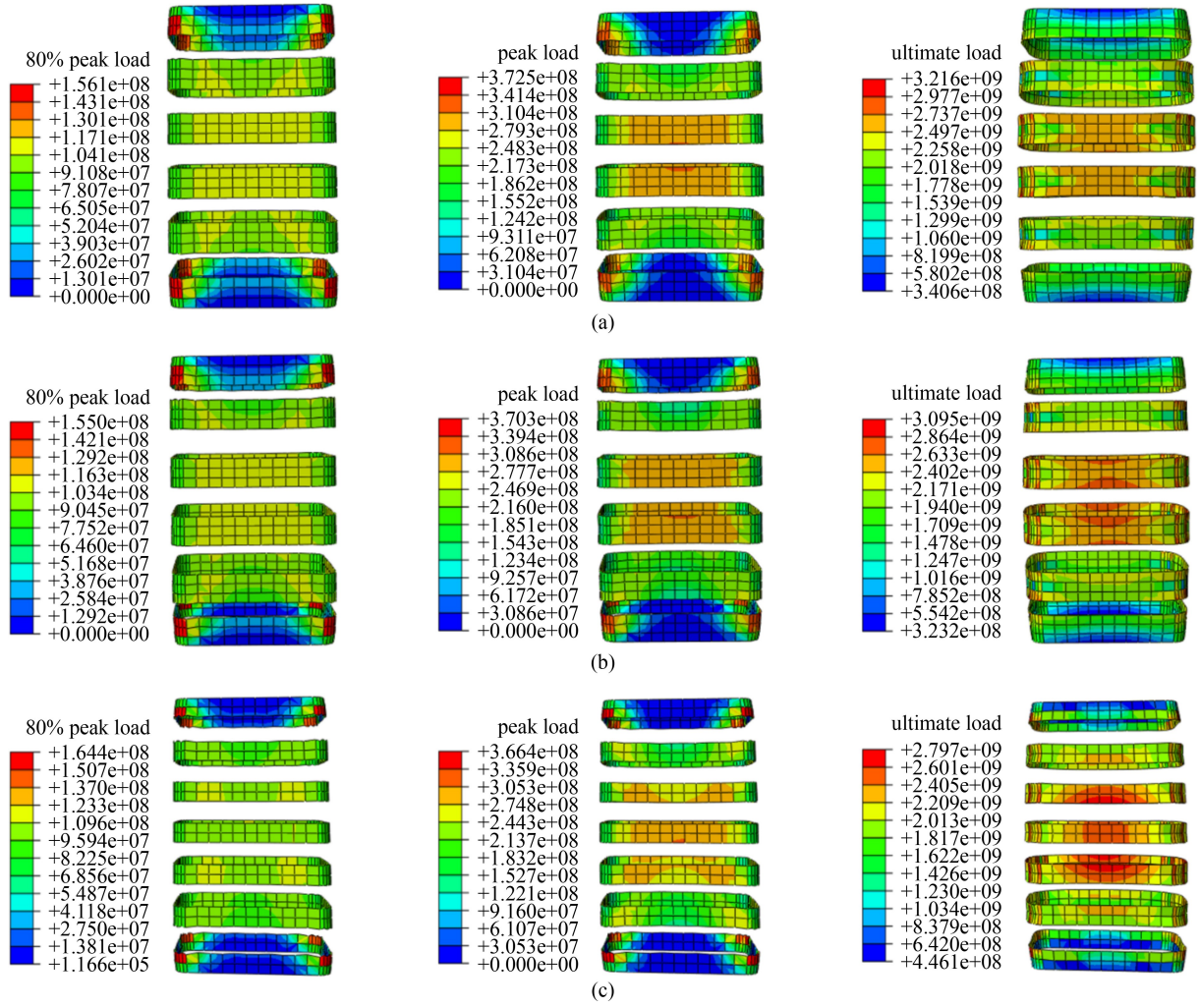

Fig. 18 Maximum principal stress nephogram of CFRP strips in the typical specimens: (a) stress nephogram of CFRP strips in CFRP-SRRC-3 specimen; (b) stress nephogram of CFRP strips in CFRP-SRRC-4 specimen; (c) stress nephogram of CFRP strips in CFRP-SRRC-7 specimen.

Table 8 Comparison between the test values and simulation values of peak loads

parameter analysis	specimen number	parameter levels	test values（kN）	numerical values（kN）	relative error
replacement rate of RCA	CFRP-SRRC-1	0	2780.19	2647.67	4.77%
	CFRP-SRRC-2	50%	2656.80	2531.59	4.95%
	CFRP-SRRC-3	100%	2647.06	2507.82	5.55%
CFRP strips spacing	CFRP-SRRC-5	25 mm	2669.73	2573.13	2.87%
	CFRP-SRRC-3	40 mm	2647.06	2507.82	5.55%
	CFRP-SRRC-4	50 mm	2635.97	2422.23	8.82%
CFRP strips width	CFRP-SRRC-7	35 mm	2531.33	2392.82	5.79%
	CFRP-SRRC-3	50 mm	2647.06	2507.82	5.55%
	CFRP-SRRC-6	65 mm	2656.97	2668.76	0.44%
	CFRP-SRRC-3	C40	2647.06	2507.82	5.55%
RAC strength	CFRP-SRRC-8	C50	3113.72	2739.16	13.67%
	CFRP-SRRC-9	C60	3251.55	3005.63	8.18%

(3) Based on Fig. 20(c), it shows that the CFRP strips layers have some certain impact on the deformation performance and axial bearing capacity of columns, and the axial bearing capacity gradually increases with the

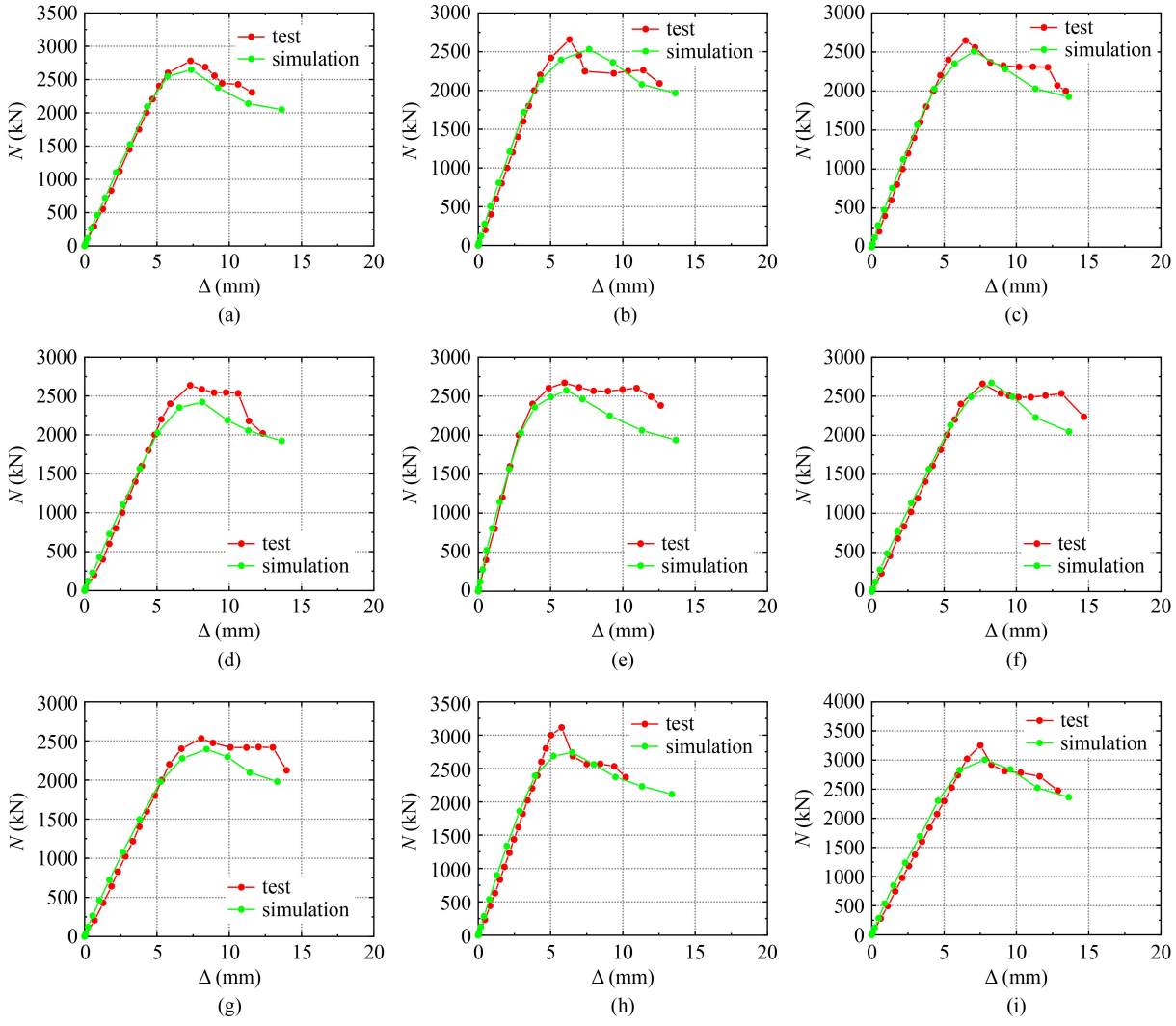

Fig. 19 Comparison of the test curves and numerical curves of specimens: (a) CFRP-SRRC-1; (b) CFRP-SRRC-2; (c) CFRP-SRRC-3; (d) CFRP-SRRC-4; (e) CFRP-SRRC-5; (f) CFRP-SRRC-6; (g) CFRP-SRRC-7; (h) CFRP-SRRC-8; (i) CFRP-SRRC-9.

Table 9 Axial bearing capacity of the columns on the numerical simulation under different parameters

specimen number	profile steel strength	chamfer radius of column R (mm)	CFRP strips width d (mm)	CFRP strips layers n	bearing capacity (kN)
CFRP-SRRC-FEA-1	Q235	20	50	2 layers	2507.82
CFRP-SRRC-FEA-2	Q345	20	50	2 layers	2826.93
CFRP-SRRC-FEA-3	Q390	20	50	2 layers	2980.63
CFRP-SRRC-FEA-4	Q235	0	50	2 layers	2433.83
CFRP-SRRC-FEA-5	Q235	10	50	2 layers	2469.84
CFRP-SRRC-FEA-6	Q235	30	50	2 layers	2673.93
CFRP-SRRC-FEA-7	Q235	20	0	0 layer	2319.93
CFRP-SRRC-FEA-8	Q235	20	10	2 layers	2330.51
CFRP-SRRC-FEA-9	Q235	20	20	2 layers	2344.76
CFRP-SRRC-FEA-10	Q235	20	35	2 layers	2392.82
CFRP-SRRC-FEA-11	Q235	20	40	2 layers	2439.10
CFRP-SRRC-FEA-12	Q235	20	65	2 layers	2668.76
CFRP-SRRC-FEA-13	Q235	20	50	1 layer	2428.82
CFRP-SRRC-FEA-14	Q235	20	50	3 layers	2617.45
CFRP-SRRC-FEA-15	Q235	20	50	4 layers	2696.07

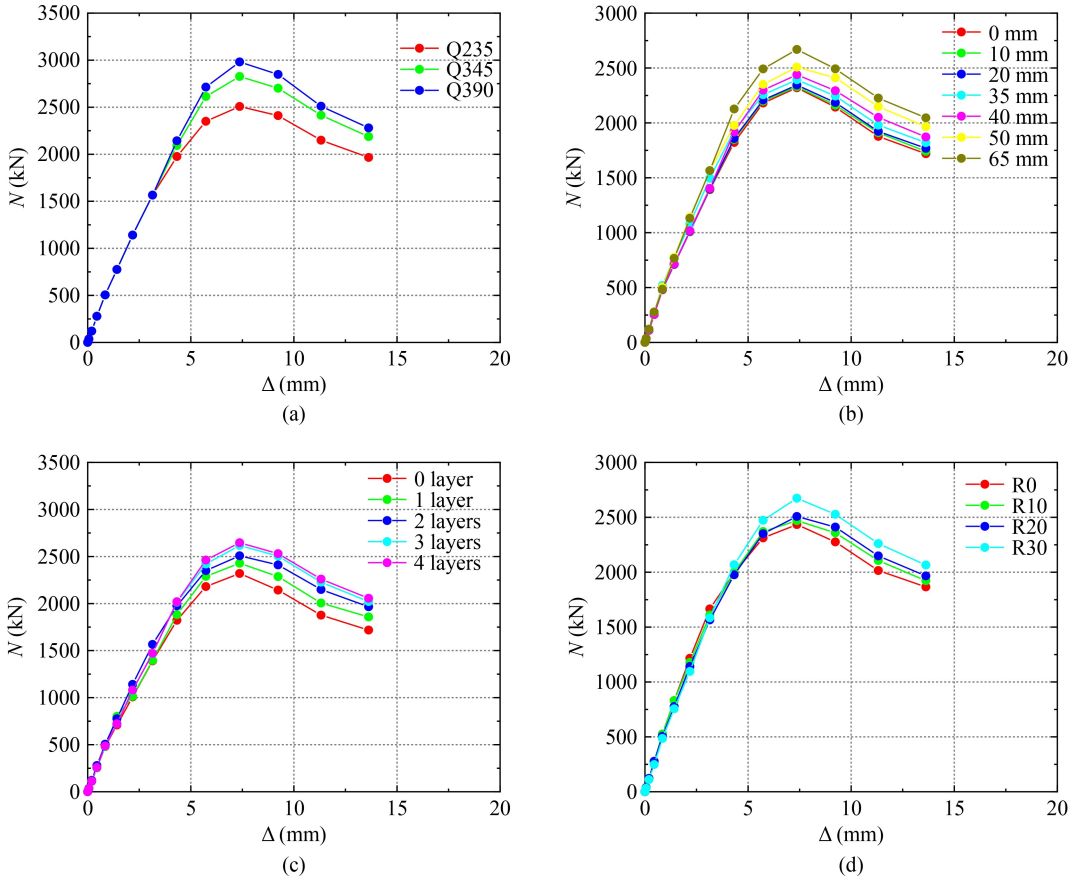

Fig. 20 Load-displacement curves of the columns under different parameters: (a) profile steel strength; (b) CFRP strips width; (c) CFRP strips layers; (d) chamfer radius of cross section.

increase of CFRP strips layers. If the layers number of CFRP strips is greater than 3.0, the axial bearing capacity of the column increases little, only about 3%, so it is recommended that the layers number of CFRP strips should not exceed 3.0.

(4) From Fig. 20(d), the curves of columns are basically the same before the peak load is reached, which shows the change of chamfer radius of cross section has little impact on the initial stiffness of columns. The axial bearing capacity increases a little with the increase of the chamfer radius of cross section, and the declining stage of load-displacement curves shows a trend of first fast and then slows. When the section of column is close to a rectangle (that is, the section chamfer is very small), the axial bearing capacity is lower than that when the section of column is close to a circle (that is, the section chamfer is very large). The axial bearing capacity of column with chamfer radius of 30 mm is 9.9% higher than that of the rectangular column without chamfer radius.

5 Calculation on the axial bearing capacity of columns confined by carbon fiber reinforced plastics strips

Based on the above tests and numerical simulation, a bearing capacity correction calculation method is proposed for this kind of short column in this study, which can offer technical reference for the practical application of SRRC short columns confined by CFRP strips.

5.1 Mechanical mechanism of the columns under axial compression loading

It can be seen from the above analysis that under the action of vertical load, the profile steel and longitudinal rebars have reached the yield strength at the peak load, and RAC has also cracked, indicating that the three materials have given full play to their performance, so the vertical bearing capacity should be borne by these three materials, as shown in Eq. (26). In particular, RAC material is in three-dimensional compression state under the restraint of CFRP strips and transverse stirrup, so the effect of restraining and strengthening concrete should be calculated in the nominal axial bearing capacity of the columns, which is more accurate. Figure 21 describes the axial compressive stress diagram of SRRC short columns confined by CFRP strips.

As mentioned above, when the axial bearing capacity of columns is calculated, the restraint effect of RAC

should be considered. At present, there are few studies on the strength calculation model of SRRC columns confined by CFRP strips. However, there are a lot of research on FRP confined reinforced concrete members. This paper modified the calculation model of FRP confined reinforced concrete based on the code ACI 440.2R-08 [33]. According to the test study, it can be concluded that the mechanical properties of RAC restrained by CFRP strips are similar to ordinary concrete, as shown in Fig. 21(a). The strength model of concrete strength in FRP confined ordinary concrete is given in document [33], as follows.

$$f_{cc} = f_{co} + 3.3\psi_f k_a f_l. \tag{13}$$

where f_{cc} is the compressive strength of CFRP strips confined RAC; f_{co} is the compressive strength of unconstrained RAC; f_l is the lateral restraint force of CFRP strips, and its calculation is shown in Eqs. (22)–(23); ψ_f is the additional reduction factor of RAC strength after the restraint, and the value is 0.95; k_a is influence coefficient of section shape, and it depends on the cross-sectional area and length-width ratio h/b of the effectively restrained RAC, as shown in Eq. (18).

The above formula includes the strength of the concrete itself and the strengthening strength of FRP constraints. In addition, it also considers the adverse effect of the replacement rate of RCA in this study. Combined with the test data, the reduction factor on the replacement rate of RCA can be put forward by regression method ϕ_r [34]. Therefore, Eq. (13) is modified as follows:

$$f_{cc} = \phi_r f_{co} + 3.3\psi_f k_a f_l, \tag{14}$$

$$\phi_r = 0.88/(-0.3r^2 + 0.45r + 1), \tag{15}$$

where r is the substitution rate of RCA.

Besides, the welded transverse stirrups were adopted in SRRC short columns and it can be seen that stirrups played a strong restraint role in maximum load from the load-strain curves of stirrups, which is conducive to enhance the axial bearing capacity of SRRC columns. However, the influence of stirrups on concrete strength is not considered in ACI. The transverse binding force f_{stl} of stirrups on columns is considered in this study, as shown in Eq. (17). Figure 20(c) shows a simplified model diagram for the calculation of CFRP strips and stirrups constrained RAC. Therefore, Eq. (14) can be modified, as shown in Eq. (16).

$$f_{cc} = \phi_r f_{co} + 3.3\psi_f k_a f_l + f_{stl}, \tag{16}$$

$$f_{stl} = \frac{n_{st} f_{yt} A_{st}}{s b_c}, \tag{17}$$

$$k_a = \frac{A_e}{A_c}\left(\frac{b}{h}\right)^2, \tag{18}$$

where n_{st} is the number of stirrup legs; A_{st} is the section area of stirrups; f_{yt} is the yield strength of stirrups; s is the spacing of stirrups; b_c is the center line distance of stirrups; A_c and A_e are the section area and effective restraint area of columns, their ratio is shown in Eqs. (19)–(20).

In addition, due to the rectangular cross-section of

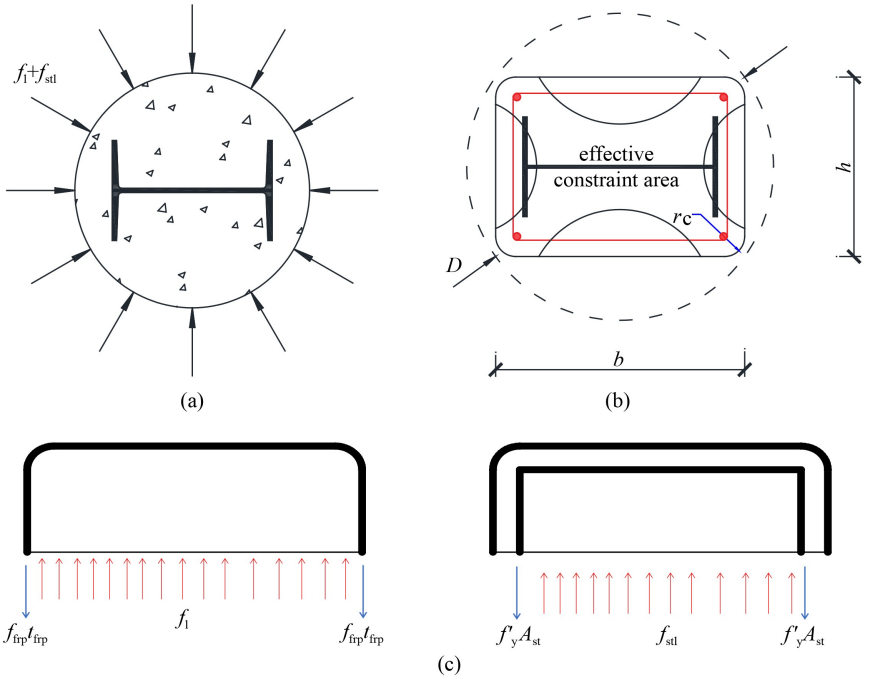

Fig. 21 Axial compressive stress of the SRRC short columns confined by CFRP strips: (a) confined RAC; (b) equivalent circular section of square section; (c) stress diagram of CFRP and stirrups.

SRRC short columns in this research, the lateral pressure of CFRP strips on the columns is not uniform due to the stress concentration effect. When the CFRP strips wrap the columns with a circular section, the restraint stress is uniformly distributed along the periphery of columns. In view of this, in order to facilitate the calculation, the rectangular columns in this study need to be equivalent to the circular columns, as shown in Fig. 21(b). The diameter D of the equivalent circular section is calculated as Eq. (21).

$$\frac{A_e}{A_c}=\frac{1-\dfrac{\left[\left(\dfrac{b}{h}\right)(h-2r_c)^2+\left(\dfrac{h}{b}\right)(b-2r_c)^2\right]}{3A_g}-\rho_g}{1-\rho_g}, \tag{19}$$

$$A_g=hb-(4-\pi)r_c^2, \tag{20}$$

$$D=\sqrt{b^2+h^2}, \tag{21}$$

where r_c is the chamfer radius of cross-section of columns; b and h are the width and height of cross section; A_g is the total cross-sectional area of columns; ρ_g is the rate of the sum of sectional area of profile steel and longitudinal rebars to the sectional area of column.

The failure process of the specimens and the load-strain curves of the CFRP strips show that the CFRP strip plays a strong restraint role at the peak load, but it has not reached the failure state of the material. The restraint of CFRP strips produces the lateral stress f_l on RAC material in the columns, it shown in Fig. 18(c), which can be calculated by Eq. (22) in ACI [33]. Where the efficiency factor of strain $k_\varepsilon = 0.55$, ε_{fu} is the fracture strain of CFRP strips; t_f is the thickness of single-layer CFRP strips; ε_{fe} is the effective fracture strain of CFRP strips; E_f is the elastic modulus of CFRP strips.

$$f_l=\frac{2E_f n t_f \varepsilon_{fe}}{D}, \tag{22}$$

$$\varepsilon_{fe}=k_\varepsilon \varepsilon_{fu}. \tag{23}$$

The test analysis shows that with the increasing number of CFRP layers, the increase degree on the axial bearing capacity of columns decreases gradually. Therefore, considering the influence of CFRP strip layers, the correction factor μ_n of confinement effect was introduced in this study, as shown in Eq. (24), where n is the layers number of CFRP strips.

$$\mu_n=\begin{cases}1, & n=1,\\ 0.9-0.05(n-2), & n\geqslant 2.\end{cases} \tag{24}$$

Because the CFRP strips are wrapped outside SRRC short columns, the width and spacing of CFRP strips have a strong influence on the axial bearing capacity of columns, the influence coefficient k_f of CFRP strips spacing was proposed in this study. k_f is the rate of effective restraint area and the section area of RAC in the columns; s_f is the spacing of CFRP strips.

$$k_f=\frac{\left(b-\frac{1}{2}s_f\right)\left(h-\frac{1}{2}s_f\right)}{bh}k_d. \tag{25}$$

Considering the effect of CFRP strips width on SRRC short columns, the influence coefficient of CFRP strips width $k_d = 0.044e^{23d} + 0.88$ was proposed, where d is the width of CFRP strips in the columns and it is suitable for $d < 70$ mm.

5.2 Comparisons on the nominal axial bearing capacity of columns

Based on the superposition methods, the nominal axial bearing capacity of SRRC short columns confined by CFRP strips can be calculated as the following formula:

$$N_c=\mu_n k_f f_{cc} A_c + f_a A_a + f_y A_s, \tag{26}$$

where N_c is the nominal axial bearing capacity of columns; μ_n is influence coefficient of CFRP constraint layers; k_f is influence coefficient of CFRP strips spacing; f_{cc} is the compressive strength of RAC confined by CFRP strips; A_c is the cross-sectional area of RAC confined by CFRP strips; f_a is the compressive strength of profile steel; A_a is the section area of profile steel; f_y is the compressive strength of longitudinal rebars; A_s is the sectional area of longitudinal rebars.

The comparison results between test values and calculated values based on the above calculation formulas are shown in Table 10. It can be obtained from Table 10 that the relative error between calculated values and test values is relatively small, with the average error of 0.971 and the standard deviation of 0.036. As a whole, the proposed calculation formulas can better meet the calculation accuracy requirements on the axial bearing capacity of SRRC short columns confined by CFRP strips.

6 Conclusions

(1) In this investigation, the failure modes of all SRRC short columns confined by CFRP strips under axial compression loading is almost the same. The profile steel first reached the yield state, and then the longitudinal rebars and transverse stirrups yielded one after another. Afterwards, RAC inside the columns was crushed, finally CFRP strips reached the ultimate tensile strain, which means that CFRP strips was broken and the columns lost its axial bearing capacity.

(2) Known from the test, the axial bearing capacity of

Table 10 Comparison between test values and calculated values on the axial bearing capacity of columns

specimennumber	r	steel strength	d (mm)	s (mm)	RAC strength	R (mm)	n	calculated values N_c (kN)	test values N_t (kN)	N_c/N_t
CFRP-SRRC-1	0%	Q235	50	40	C40	20	2 layers	2668.71	2780.19	0.960
CFRP-SRRC-2	50%	Q235	50	40	C40	20	2 layers	2514.95	2656.80	0.947
CFRP-SRRC-3	100%	Q235	50	40	C40	20	2 layers	2514.95	2647.06	0.950
CFRP-SRRC-4	100%	Q235	50	50	C40	20	2 layers	2362.99	2532.59	0.933
CFRP-SRRC-5	100%	Q235	50	25	C40	20	2 layers	2651.69	2798.73	0.947
CFRP-SRRC-6	100%	Q235	65	40	C40	20	2 layers	2609.79	2796.97	0.933
CFRP-SRRC-7	100%	Q235	35	40	C40	20	2 layers	2447.78	2510.33	0.975
CFRP-SRRC-8	100%	Q235	50	40	C50	20	2 layers	2771.22	3113.72	0.890
CFRP-SRRC-9	100%	Q235	50	40	C60	20	2 layers	3027.50	3251.55	0.931
CFRP-SRRC-FEA-1	100%	Q235	50	40	C40	20	2 layers	2514.95	2507.82	1.003
CFRP-SRRC-FEA-2	100%	Q345	50	40	C40	20	2 layers	2751.45	2826.93	0.973
CFRP-SRRC-FEA-3	100%	Q390	50	40	C40	20	2 layers	2848.20	2980.63	0.956
CFRP-SRRC-FEA-4	100%	Q235	50	40	C40	0	2 layers	2228.94	2433.83	0.916
CFRP-SRRC-FEA-5	100%	Q235	50	40	C40	10	2 layers	2416.98	2469.84	0.979
CFRP-SRRC-FEA-6	100%	Q235	50	40	C40	30	2 layers	2511.01	2673.93	0.939
CFRP-SRRC-FEA-7	100%	Q235	0	0	C40	20	0 layer	2357.64	2319.93	1.016
CFRP-SRRC-FEA-8	100%	Q235	10	40	C40	20	2 layers	2376.49	2330.51	1.020
CFRP-SRRC-FEA-9	100%	Q235	20	40	C40	20	2 layers	2400.21	2344.76	1.024
CFRP-SRRC-FEA-10	100%	Q235	35	40	C40	20	2 layers	2447.78	2392.82	1.023
CFRP-SRRC-FEA-11	100%	Q235	40	40	C40	20	2 layers	2467.65	2439.10	1.012
CFRP-SRRC-FEA-12	100%	Q235	65	40	C40	20	2 layers	2609.79	2668.76	0.978
CFRP-SRRC-FEA-13	100%	Q235	50	40	C40	20	1 layer	2419.14	2428.82	0.996
CFRP-SRRC-FEA-14	100%	Q235	50	40	C40	20	3 layers	2602.69	2617.45	0.994
CFRP-SRRC-FEA-15	100%	Q235	50	40	C40	20	4 layers	2697.01	2696.07	1.000

Note: r is the substitution rate of RCA; d is the CFRP strips width; s is the CFRP strips spacing; R is the fillet radius of column; n is the number layers of CFRP strips.

columns decreases with the increasing replacement rate of RCA, but the decrease range is relatively small, and the maximum decrease is only 4.8%. Increasing the CFRP strips width or decreasing the CFRP strips spacing can increase the axial bearing capacity and deformation of columns, and the maximum increase of bearing capacity is 10.5% and 11.4%, respectively. Besides, the axial bearing capacity of columns also enhances with the increase of RAC strength, but the deformation of columns decreases gradually.

(3) The calculation results of numerical model used in the study are in good agreement with the experimental results, which shows that the numerical model established by ABAQUS software is reasonable. The numerical model considers the adverse influence on the substitution ratio of RCA and the constraint effect of CFRP strips, and well reflects the mechanical characteristics of columns.

(4) The results of parameter analysis indicate that the axial bearing capacity of columns is greatly enhanced with the increasing strength of profile steel, and the maximum increase is 18.9%. The increasing corner fillet radius of cross section is beneficial to the bearing capacity of columns. Moreover, the bearing capacity and deformation capacity of columns increases with the increasing CFRP strips layers. Nevertheless, when the layers number of CFRP strips exceeds 3, the bearing capacity of columns is enhanced slightly. Therefore, it is proposed that when the layers number of CFRP strips is 2–3, the restraint enhancement effect on the columns is the best.

(5) Considering the influence of substitution rate of RCA and the restraint effect of CFRP strips and stirrups, the modified formulas on the axial bearing capacity of SRRC short columns confined by CFRP strips was proposed. The validity of the modified formula is verified by calculation.

(6) In general, the axial bearing capacity and ductility of SRRC short columns are greatly improved by the restraint of CFRP strips. The research results provide a way for the application of RAC material.

Acknowledgments The financial support of this work came from the

project of National Natural Science Foundation of China (Grant No. 51408485), the Natural Science Basic Research Plan in Shaanxi Province of China (Nos. 2022JM-258 and 2021JM-332), the Open Fund Project of Qinghai Provincial Key Laboratory of Plateau Green Building and Eco-community (KLKF-2021-001), and thanks a lot for the financial support of the above institutions.

References

1. Rafaela C, Rui V S, Jorge de B, Ravindra D. Use of recycled aggregates from construction and demolition waste in geotechnical applications: A literature review. Waste Management (New York, N.Y.), 2016, 49(3): 131−145
2. Tereza P, Vladimír K, Petr H. Environmental assessment of two use cycles of recycled aggregate concrete. Sustainability (Basel), 2019, 11(21): 6185
3. Zhang J H, Wu Z Y, Zhang Y D, Fang Q, Yu H F, Jiang C L. Mesoscopic characteristics and macroscopic mechanical properties of coral aggregates. Construction & Building Materials, 2021, 309(22): 125125
4. Liu C Q, Wei X D, Lu Z, Wu H D, Yang Y L, Chen L Y. Studies on passive flexible protection to resist landslides caused by the May 12, 2008, Wenchuan earthquake. Structural Design of Tall and Special Buildings, 2017, 26(11): e1372
5. Vito F, Carlos M, Mirian V L. Effect of recycled concrete aggregate (RCA) on mortar's thermal conductivity susceptibility to variations of moisture content and ambient temperature. Journal of Building Engineering, 2021, 43(11): 103208
6. Sun C, Chen Q, Xiao J, Ge W. Study on aggregate interlock behavior of pre-cracked recycled aggregate concrete without stirrups. Journal of Building Engineering, 2021, 39(7): 102257
7. Silva R V, de Brito J, Dhir R K. Fresh-state performance of recycled aggregate concrete: A review. Construction & Building Materials, 2018, 178(7): 19−31
8. Zhang J H, Li C, Ding L, Li J. Performance evaluation of cement stabilized recycled mixture with recycled concrete aggregate and crushed brick. Construction & Building Materials, 2021, 296(8): 123596
9. Du Y B, Zhao Z Q, Xiao Q, Shi F T, Yang J M, Gao P W. Experimental study on the mechanical properties and compression size effect of recycled aggregate concrete. Materials (Basel), 2021, 14(9): 2323
10. Syed M S K, Muhammad J M, Wu Y F, Indubhushan P, Zhou Y W, Feng X. Influence of different treatment methods on the mechanical behavior of recycled aggregate concrete: A comparative study. Cement and Concrete Composites, 2019, 104(11): 103398
11. Sepani S, Gregory L, Olivia M, Vivian W Y T, Kang W H. Recycle concrete in structural Applications for sustainable construction Practices in Australia. Procedia Engineering, 2017, 180(4): 751−758
12. Dong H Y, Li Y N, Cao W L, Guo Y L. Seismic behavior of full-scale steel reinforced recycled concrete columns under high axial compression ratio. Structures, 2021, 29(2): 1882−1897
13. Ma H, Jia C J, Xi J C, Dong J, Zhang X C, Zhan Y L. Cyclic loading test and nonlinear analysis on composite frame consisting of steel reinforced recycled concrete columns and steel beams. Engineering Structures, 2021, 241(8): 112480
14. Huang W, Fan Z C, Shen P L, Lu L N, Zhou Z. Experimental and numerical study on the compressive behavior of micro-expansive ultra-high-performance concrete-filled steel tube columns. Construction & Building Materials, 2020, 254(9): 119150
15. Ma H, Xi J C, Zhao Y L, Dong J K. Mechanical behaviour of composite columns composed of RAC-filled square steel tube and profile steel under eccentric compression loads. Steel and Composite Structures, 2021, 38(1): 103−120
16. Dong J, Ma H, Liu Y H, Guo T T. Numerical analysis and axial bearing capacity of composite columns with recycled aggregate concrete-filled steel tube and profile steel. Arabian Journal for Science and Engineering, 2020, 45(1): 3581−3598
17. Ma H, Dong J, Hu G B, Liu Y H. Axial compression performance of composite short columns composed of RAC-filled square steel tube and profile steel. Journal of Constructional Steel Research, 2019, 153(2): 416−430
18. Ma H, Dong J, Liu Y H, Guo T T. Compressive behaviour of composite columns composed of RAC-filled circular steel tube and profile steel under axial loading. Journal of Constructional Steel Research, 2018, 143(4): 72−82
19. Zhao T F. Bearing capacity studies on square steel tube confined steel reinforced concrete column under eccentric load. Advances in Civil Engineering, 2020, 2020(5): 4212049
20. Vivian W Y, Xiao J, Liu S, Chen Z. Behaviors of recycled aggregate concrete-filled steel tubular columns under eccentric loadings. Frontiers of Structural and Civil Engineering, 2019, 13(3): 628−639
21. Cao Y G, Liu M Y, Wu Y F. Effect of low strain rate on the axial behavior of concrete in CFRP-confined circular cylinders. Construction & Building Materials, 2020, 255(9): 119351
22. Wang Y L, Cai G C, Amir S L, Danièle W, Konstantinos D T, Ran J H. Monotonic axial compressive behaviour and confinement mechanism of square CFRP-steel tube confined concrete. Engineering Structures, 2020, 217(8): 110802
23. Liu X, Wu T, Chen H X, Liu Y. Compressive stress-strain behavior of CFRP-confined lightweight aggregate concrete reinforced with hybrid fibers. Composite Structures, 2020, 244(7): 112288
24. Yasmin M, Wassel A B, Ahmed A. Seismic retrofitting of severely damaged RC connections made with recycled concrete using CFRP sheets. Frontiers of Structural and Civil Engineering, 2020, 14(2): 554−568
25. Chen G M, He Y H, Jiang T, Lin C J. Behavior of CFRP-confined recycled aggregate concrete under axial compression. Construction & Building Materials, 2016, 111(5): 85−97
26. GB/T-25177-2010. Recycled Coarse Aggregate for Concrete. Beijing: China Standards Press, 2010 (in Chinese)
27. CECS146:2003. Technical Specification for Concrete Structures Strengthened with Carbon Fiber Sheet. Beijing: China Planning Press, 2003 (in Chinese)
28. Ma H, Wu Y N, Huang C, Zhao Y L. Mechanical properties and bearing capacity of CFRP configured steel reinforced recycled concrete columns under axial compression loading. Structural

Engineering and Mechanics, 2021, 79(4): 451−472
29. Xiao J Z. Experimental study on complete stress−strain curve of recycled concrete under uniaxial compression. Journal of Tongji University (Natural Science Edition), 2007, 52(11): 1445−1449
30. GB 50010-2015. Code for Design of Concrete Structures. Beijing: China Construction Industry Press, 2015 (in Chinese)
31. Xiao J Z, Lan Y. Experimental study on uniaxial tensile properties of recycled concrete. Journal of Building Materials, 2006, 51(2):154–158 (in Chinese)
32. Hashin Z. Failure Criteria for unidirectional fiber composites. Journal of Applied Mechanics, 1980, 47(2): 329−334
33. Realfonzo R, Aa VV. ACI 440.2R-08. Guide for the Design and Construction of Externally Bonded FRP Systems for Strengthening Concrete Structures. Michigan: American Concrete Institute, 2008
34. Xiao J Z, Yang J, Huang Y J, Wang Z P. Experimental study on axial pressure of recycled concrete with steel tube restraint. Journal of Architectural Structure, 2011, 32(6):92–98 (in Chinese)
35. Zeng J J, Guo Y C, Gao W Y, Li J Z, Xie J H. Behavior of partially and fully FRP-confined circularized square columns under axial compression. Construction & Building Materials, 2017, 152(10): 319−332
36. Zeng J J, Guo Y C, Gao W Y, Chen W P, Li L J. Stress−strain behavior of concrete in circular concrete columns partially wrapped with FRP strips. Composite Structures, 2018, 200(9): 810−828
37. Chrzanowski M, Odenbreit C, Obiala R, Bogdan T, Degée H. Effective bending stiffness of steel−concrete composite columns with multiple encased steel profiles. Journal of Constructional Steel Research, 2021, 181(6): 106607
38. Liang J F, Lin S Q, Li W, Liu D W. Axial compressive behavior of recycled aggregate concrete-filled square steel tube stub columns strengthened by CFRP. Structures, 2021, 29(2): 1874−1881